Real-time Optimal Battery Thermal Management System Controller for Electric and Plug-in Hybrid Electric Vehicles

by

Yasaman Masoudi

A thesis
presented to the University of Waterloo
in fulfillment of the
thesis requirement for the degree of
Master of Applied Science
in
Systems Design Engineering

Waterloo, Ontario, Canada, 2017

I hereby declare that I am the sole author of this thesis. This is a true copy of the thesis, including any required final revisions, as accepted by my examiners.

I understand that my thesis may be made electronically available to the public.

Abstract

The objective of this thesis is to propose a real-time model predictive control (MPC) scheme for the battery thermal management system (BTMS) of given plug-in hybrid electric and electric vehicles (PHEV/EVs). Although BTMS control in its basic form can be well represented by a reference tracking problem, there exists only little research in the literature taking such an approach. Due to the importance of a prediction component in thermal systems, here the BTMS controller has been designed based on MPC theory to address this gap in the literature. Application of the controller to the baseline vehicles is then examined by several simulations with different optimization algorithms.

By comparing the results of the predictive controller with those of the standard rule-based (RB) controller over a variety of driving scenarios, it is observed that the predictive controller significantly reduces the power consumption and provides a better tracking behaviour. Integrating trip prediction into the control algorithm is particularly important in cases such as aggressive driving cycles and highly variable road-grades, where the standard BTMS scheme does not perform as effectively due to the load current profile.

Moreover, based on the simulation results, the designed controller is observed to have a turnaround time between $10\,\mu s$ to $1\,ms$, and is thus applicable to the real-time automotive systems.

Prosperity of the proposed BTMS control methodology paves the way for the use of model-based (MB) thermal management techniques, not only in future electric propulsion vehicles but also in a wide range of upcoming battery-based devices.

Acknowledgements

I would like to thank all the people who made this possible, mainly my supervisor, Professor Azad, for his great patience and endless support. Also, my amazing friends at the Motion Research Group, specially Dr. Joydeep Banerjee, Amer Keblawi, and Dr. Ehsan Samadani, without the valuable time of whom this could not have happened.

Dedication

To the beautiful souls of ladies who have not been given a chance to bloom.

Table of Contents

List of Tables

List of Figures

Nomenclature

AC Air Conditioning
BEV Battery Electric Vehicle
$BFGS$ Broyden-Fletcher-Goldfarb-Shanno
$BTMS$ Battery Thermal Management System
CAN Controller Area Network
CGM Conjugate Gradient Method
DP Dynamic Programming
DSM Direct-step Method
ECM Equivalent Circuit Model
ECU Electronic Control Unit
EOL End-of-life
ESS Energy Storage System
EV Electric Vehicle
FEM Finite Element Method
HIL Hardware-in-the-loop
IP Interior-point
KKT Karush-Kuhn-Tucker
MB Model-based
MBD Model-based Design
MIL Model-in-the-loop
MPC Model Predictive Control
NLP Nonlinear Programming
$NMPC$ Nonlinear Model Predictive Control
OCP Optimal Control Problem
PD Positive Definite
$PHEV$ Plug-in Hybrid Electric Vehicle
PMP Pontryagin Minimum Principle
RB Rule-based

RHS Right Hand Side
SOC State of Charge
SQP Sequential Quadratic Programming

Chapter 1

Introduction

Battery electric and plug-in hybrid electric vehicles are not supporting actors any more; the global air-pollution crisis has now challenged the automotive industry to give these vehicles more important roles in the transportation realm. Billions of miles have been driven in full EV mode world-wide [59], with the battery being the only energy supplier. The critical role of the battery, as one of the most important components in EVs and PHEVs, has lead to the assignment of significant resources to battery-related research. This research shows that battery's life and performance are functions of its temperature; therefore, developing the right BTMS becomes profoundly important. So far, mechanisms applied in this regard mostly include rule-based approaches, which are cost-effective, yet may have shortcomings.

This thesis focuses on the design and implementation of a BTMS controller using an MPC approach, and discusses the benefits that such an approach suggests.

The remainder of this introduction is organized as follows: first the core motivation as well as the ultimate objective in this research are discussed in more depth. Second, the problem statements for each of the platforms applied in this study are given. Third, the contributions are stated. Finally, the thesis organization is provided.

1.1 Motivation and Research Objective

Application of RB controllers in the hybrid vehicles has been extensive [85]. The automotive industry has often applied RB strategies to actuate mechanisms, such as battery cooling/heating circuits. The applied RB controllers can be on-off (or thermostat) or have

several rules and maps in them to improve their performance [53]. Sometimes such rules can be obtained based on the external inputs to the system, like power demand [85], but more often they are extracted from a great deal of experimental data. In many trip scenarios, they can take care of the control problem very well; simulations demonstrate that RBs could perform well for a variety of conditions, such as particular urban and highway cycles [85]. In certain driving scenarios they have even shown results with only 1% deviation from those of the dynamic programming (DP) [47].

To provide more accuracy, the controller parameters, such as the switching thresholds, are often calibrated using optimal methods such as DP [62]. This calibration is heavy [79], and takes time and effort. Also, as the calibration is based on certain driving scenarios, it may not adapt well to a new scenario. Moreover, possible changes in the system architecture could disqualify all or part of the rules.

The above-mentioned problems with the RB strategies spark the search for other control algorithms. One way could be to systematically incorporate the model information into the control strategy by using an MB approach. Model-based design (MBD) is a very popular methodology for developing controllers in the industry [21]. As the vehicle control-problems are complicated [43], the automotive industry has started investing in the MBD to handle them. Different types of MB controllers are applied in the electrified vehicles [79]; they could be merely bench-marks providing the optimal solution of the problem (like [95]) or real-time algorithms, such as [79].

As stated above, RB methods take expensive calibration, and the resulting tuned parameters may just work for special cases. MB optimization methods can address this issue[80]. Also, unlike the RB approaches, MB methods do not require repetition of the whole calibration process when the system configuration is subject to changes, and the applied changes could be directly addressed. Additionally, the MB controllers demonstrate a higher performance than that of the rule-based controllers [79] [80]. Another important consideration is the critical role of the physical constraints, as they impact the BTMS control problem behaviour. Fortunately, MB approaches can handle the hard constraints [79].

MB techniques can be combined with optimization approaches. As such, an accurate objective function is defined and minimized, and the controller could achieve the requirements [43]. This method can take care of problems with multiple objectives [61] and also handle hard and soft constraints, either on the states or input [43]. Moreover, many complicated problems, including those subject to transient operation of actuators, could be addressed [22].

Based on the level of trip knowledge in their architecture, MB optimization algorithms

can be online or offline [79]. In the PHEV context, an offline global optimization problem, like one formulated using Pontryagin minimum principle (PMP), could be turned into a local optimization problem to be implemented online [86]. Online MB optimization approaches could not only address the drawbacks of RBs, but also facilitate real-time implementations; one such method is MPC.

MPC is a real-time MB technique, and thus is applicable in the automotive industry. It provides a near optimal solution for the tracking problem, where its constraint handling ability ensures that the states and inputs remain within the admissible ranges. As for this thesis, it is worth mentioning that the prediction component of the MPC architecture can provide prior knowledge of the thermal-system behaviour, and thus helps to make more intelligent decisions in terms of thermal management.

Despite the importance of BTMS, little research has been conducted exploring the BTMS problem from a feed-back control perspective; PMP has been applied for BTMS control[20], but MPC-based BTMS has not been suggested in the literature. Therefore, the *objective* of this thesis is to formulate the BTMS problem using an MPC-based controller, to address this gap in the literature.

1.2 Problem Statement

As mentioned above, the focus in the current study is on designing online MB controllers for battery thermal management in PHEV and EVs. These controllers should be capable of regulating the temperature in the most severe trip scenarios. Also, the BTMS control problem is multi-objective, and there are hard constraints on the states and inputs. As a result, the problem is formulated as an MPC problem. To address the different technical details in the layout of the PHEV and EV platforms, the problem statement section is divided into two separate categories: PHEV and EV. There are specific considerations to be taken into account in each of the platforms, and the problem is stated differently in each case. As it it will be explored later, these considerations could include a different range of variables, from the available measurement signals to the drawbacks in each of the designs.

1.2.1 PHEV

In PHEVs, a battery is not the only power source, yet it is very important to ensure that its temperature is regulated well. Manufacturers have been using different approaches to satisfy this regulation; these approaches will be studied in more detail in Chapter 2.

For the baseline PHEV, namely the Toyota plug-in Prius, the goal is to first exploit the system potential with the current actuators and then modify the system without making any costly changes. By using an MB approach, this can be done by merely refining the control laws which are executed by the actuators, fans in this case study. Making further changes leads to excessive cost whereas to suit the industry needs, the key factor for this design is to be cost-effective.

First a DP method is used to investigate the maximum potential of the existing system. In the critical situations, also several simulations are conducted with the fan on all the time. The MPC controller is then implemented to both regulate the temperature and minimize the electric power consumption. To evaluate the controller, model-in-the-loop (MIL) simulations are conducted providing an understanding of the system's behaviour. Then the hardware-in-the-loop (HIL) experiments are done in order to examine the simulation time. As for the simulation model, a high-fidelity model of the system is developed, which is then reduced to give a second model proper for controller design.

1.2.2 EV

In this case, the focus is on the investigation of the MPC potential for BTMS in the baseline EV, namely the Toyota RAV4 EV. The BTMS in EVs is very important as the temperature identifies their driving range [74]. Here, the problem is formulated as a reference-temperature tracking problem, where a minimum final state of charge (SOC) is also considered as an optimization objective to increase the vehicle range.

As the main focus in this thesis is on PHEV, the research on EVs is just a preliminary study, and further future work could clarify more details.

1.3 Contributions

The most important contribution of this research is applying the model-predictive approach to BTMS controller design. In a nutshell, the main contributions of this thesis can be classified as follows:

BTMS Controller Design for PHEVs

- Development of a high-fidelity model for the PHEV energy storage system (ESS), based on a proper heat transfer model.

- Design of MPC-based BTMS controllers for PHEVs, which add the prediction component to the system, and therefore provide more intelligent decisions.
- Evaluation of MPC-based BTMS controllers using MIL simulations and HIL experiments.

BTMS Controller Design for EVs

- Design of MPC-based BTMS controllers for EVs.

1.4 Thesis Organization

The rest of this thesis is structured as follows: Chapter 2 reviews the existing literature in the most relevant areas, i.e. Li-ion batteries, battery thermal management systems, battery thermal management controllers, and optimal control approaches. Chapter 3 shows the procedure of developing the thermal management model, including the applied battery model and actuator model, for each of the baseline PHEV and EV platforms. Chapter 4 describes the applied control methodologies. It starts with an explanation of the detailed steps of implementing the nonlinear model predictive (NMPC) controller. It then adds other methods such as Dynamic Programming, linear MPC, and PID, as benchmark. Chapter 5 evaluates the controller performance: discussing the results of the MIL simulations and HIL experiments under a variety of simulation scenarios, it explicitly examines each of the controllers. Finally, Chapter 6 concludes this research. Given the outcomes of this thesis along with the previous work on the BTMSs, it then suggests the future research possibilities.

Chapter 2

Literature Survey and Background

To gain a complete view of the field, five broad areas in the literature had to be considered. First, battery models applied in similar research, and thus applicable to this study, were surveyed. Second different cooling/heating systems, implemented for vehicle-battery thermal management, were explored. Next, literature addressing feedback-control methodologies for BTMS was researched. As it will be demonstrated, there were limited studies based on feedback control; and one of the goals of this thesis is to fill this gap. Afterwards, MPC and its application were examined. Finally, research regarding HIL test benches was reviewed to create an accurate method of evaluation for the controller.

2.1 Battery Models

Importance of batteries has led to a great deal of literature regarding different characteristics of batteries such as electrochemical behaviour and degradation models. The most pertinent studies to this thesis focused on thermal and electrical battery models, specifically on how they affect the current drawn from the battery and therefore battery temperature. Heat generation, the key phenomenon connecting thermal and electrical battery behaviours, was also an important consideration.

2.1.1 Cell Type and Structure

Before discussing the thermal models, the common cell structures should be investigated, and we should limit our focus to those that can be applied in this research.

Due to advantages such as reduced weight and cost, lithium-ion batteries have now replaced nickel metal batteries in most electrified platforms, including the baseline vehicles of this research [12].

A battery pack consists of multiple battery modules, each of which contains battery cells organized in a certain structure. The three most common cell structures are prismatic, cylindrical, and pouch [77], as illustrated in Figure 2.1. In this study, cylindrical Li-on cells in a staggered layout are considered [99].

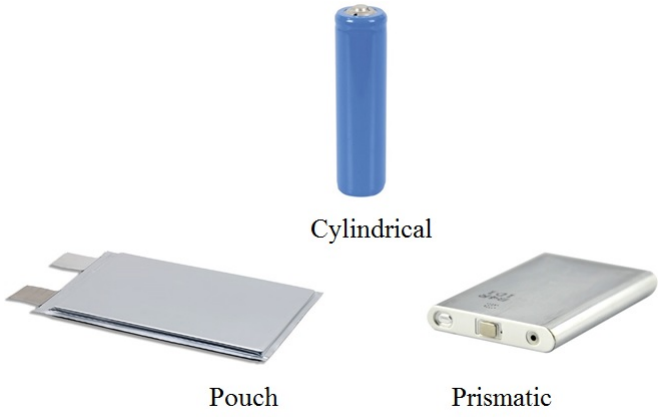

Figure 2.1: Different cell layouts.

2.1.2 Thermal Models

There exist different models addressing the thermal behaviour of the batteries. These models can get into so much detail, or merely provide a broad image of the thermal behaviour. Depending on the specific application and type of the study, one could choose a suitable model with the required level of accuracy. To see how different ranges of models with different degrees of complexity, from a complicated chemical to a simplified lumped mass model, exist, we take a look at some of the models. This way, we would gain the required background, and it becomes clear why the models that we have applied in this research make sense. Here the goal is to get familiar with some of the methods that have been applied for battery modelling to illustrate some examples for this general topic.

Electrochemical models of the battery focus on the chemical reaction inside the battery cells. Such models provide very accurate knowledge of the temperature distribution in a

cell; however, they may not be an appropriate choice for automotive applications, because of their high computational effort [77]. An example of the electrochemical models is the model for Li-ion batteries offered by Gu [42]. Finite element could also be applied to illustrate temperature distribution within a battery pack. As an example, using the finite element method (FEM), Ma [63] proposed an electro-thermal model for cylindrical Li-ion battery cells. Following a different approach, Shi [82] developed a multi-node thermal network model of the Li-ion packs. This low order model was then validated using experimental data, and proven to be applicable to the PHEV BTMS. In the meantime, Yuksel [99] used the heat transfer formulation for a staggered bank of tubes to model a Li-ion battery pack with cylindrical cells. Another type of battery model is the physics-based model, offered and validated by Pesaran [60]. There exist simplified lumped-parameter thermal battery-models. Facilitating faster simulations, such models suit automotive applications very well, and have been often applied for research in the automotive area [90].

2.1.3 Equivalent Circuit Models

Equivalent circuit models (ECMs) can represent the electrical behaviour of the battery. They adapt well to automotive-application time requirements as they don't impose excessive computational complexity.

There are different types of ECMs, such as R_{int} model, RC model, Thevenin model, and dual polarization model [45]. Based on the objectives of a study, any of these models could be applied to show the plant behaviour.

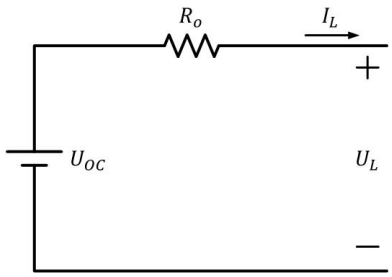

Figure 2.2: R_{int} model.

Here, the electrical control oriented models for both of the target vehicles are R_{int} models. Moreover, the Autonomie model is applied as the electrical high fidelity model in the PHEV. It comprises of R_{int} model with its parameters as maps.

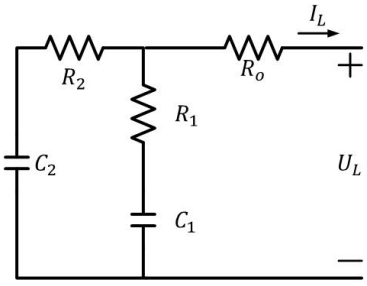

Figure 2.3: RC model.

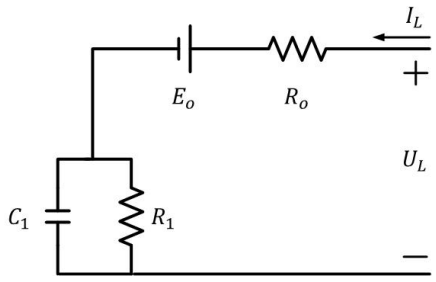

Figure 2.4: Thevenin model.

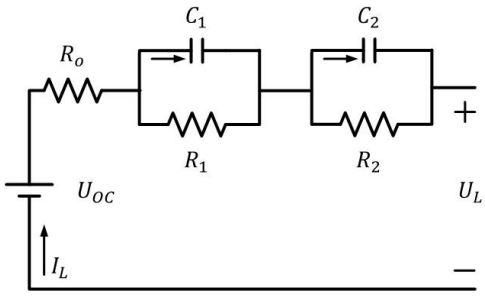

Figure 2.5: Dual polarization model.

2.1.4 Heat Generation

One important phenomena is the heat generation, as the factor leading to temperature increase in first place. Different sources are resulting in the heat generation [52] [44], and therefore a variety of models have been suggested based on which of the sources are being considered. Here, only joule heating is considered, which is the heat generated due to the thermal resistance in the battery cells, and contribute to the heat generation the most.

2.2 Battery Thermal Management Systems

Battery life is one of the main threats to the market of the electrified vehicles [71]. As it is undeniably dependent on the battery temperature [56], state-of-the-art BTMSs are essential to maintain the customers. Different thermal management techniques are applied in the auto industry; indeed, the proper technique is designed based on the functional requirements and operating conditions for each particular application. In this section, different categories of BTMSs are investigated. Based on this categorization, the BTMS design criteria and procedure are explained. Next, the relevant BTMS-modelling ideas are addressed.

2.2.1 Different types of BTMSs

BTMSs can be categorized based on different aspects; they can either facilitate only cooling or facilitate both cooling and heating. They may be liquid-based or air-based, active or passive, and direct or indirect. They may also apply parallel or series flow. Each technique has pros and cons, making it proper for certain applications [72]. In the following, these methods are briefly explained:

- **Cooling BTMS versus Cooling/heating BTMS:** The operating condition, such as climate, identifies if cooling is enough, or if both cooling and heating are necessary. EVs first started in California's warm weather, thus heating was not necessary [72]. To be applicable in cold climates, EVs were then equipped with a heater or changed so that they could use the heat generated by the electronics components. HEVs, meanwhile, could use the heat generated by the engine [72].

- **Air-based or liquid-based BTMS:** In terms of the heat transfer medium, the BTMSs are either air-based or liquid-based. Liquid-based mechanisms are often more complicated and have a better performance than that of the air-based systems [72]. Moreover, the smaller air density of the air results in a greater flow-rate and power consumption in the air-based BTMSs [56].

- **Direct versus indirect BTMS:** in a direct thermal management mechanism the flow is directly exposed to the cooling/heating-circuit actuators, as opposed to an indirect mechanism where the heat transfer is provided through a medium flow. Indirect mechanisms can be found in a variety of thermal management systems, from a refrigeration cycle [4] to a solar water heating mechanism [5].

- **Passive or active BTMS:** *passive thermal management system* could refer to a thermal management system working based on the natural heat transfer phenomena, namely radiation, conduction, and natural convection. Based on this definition, heat sinks or pipes can be part of a passive mechanism; however, actuators are not allowed [11]. All other systems, suggesting forced convection, are considered as active.

  A second definition of passive BTMS has been applied as well [72]; From this definition, BTMS is called passive when no additional heating/cooling mechanism or component is provided inside the BTMS circuit to heat/cool down the flow. Before exchanging heat with the battery pack, the flow may have been pre-conditioned, as it will be clarified later, by the vehicle heating or air conditioning (AC) system [72]; however, as pre-conditioning is not a part of the BTMS circuit, it does not violate this definition. Also, all other thermal mechanisms, such as those with the refrigeration cycles, are active due to this definition [72][98].

  Overall, the passive mechanism, considering both definitions, is cost effective and less complicated; therefore, if it meets the system requirements, it would be preferred to the active system. We consider the latter definition over the course of this thesis.

  In the passive air-based BTMSs, either ambient or cabin air is used for cooling. The ambient air, however, was more applied in the earlier designs of EVs and HEVs as they were meant to work in mild climate [72]. If the cabin air is used, AC/heating system being ON counts as the so-called pre-conditioning. It not only increases the quality of the thermal management [60], but also improves the performance of the electrified vehicles [19].

  Although passive systems are usually air-based, there exist liquid-based passive systems. They, however, are restricted in that they work the best for mild ambient-temperature ranges [72]. In this research, we focus on air-based passive systems which are more common.

  Figure 2.6 shows a passive cooling mechanism prevalently applied in hybrid vehicles; the outside or cabin air is drawn into the battery pack area through the fan, to cool the battery down. After going through the battery modules, the warm air is exhausted out.[1] In Toyota Prius 2nd generation such a system is used to cool down the battery with the cabin air [13]; in this case it has been observed that keeping the AC system ON in warm temperatures, as a pre-conditioning strategy, boosts the quality of battery cooling [3].

  It is worth mentioning that in most of the active battery thermal management sys-

[1] In some passive mechanisms, however, this air is fed back to the cabin [72]

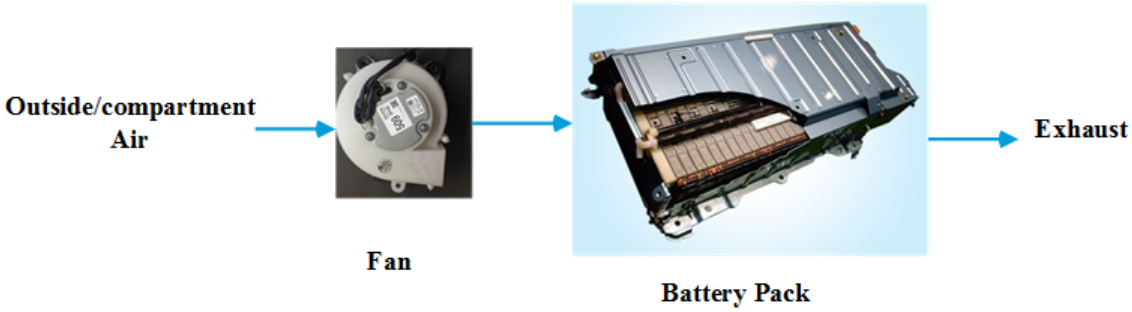

Figure 2.6: A passive cooling system. The fan sucks air from outside or the passenger compartment into the battery pack, and the warmed air is exhausted [13].

tems the AC circuit is used for battery cooling as well [13] [90]. There are, however, other cases where the engine coolant facilitates the battery tempering [72].

Figure 2.7 shows a typical refrigeration cycle applied for active BTMS in EV and PHEVs. As illustrated, the main components include compressor, condenser, expansion valve, filter receiver-drier, and evaporator. Such an approach is the foundation for the BTMS design in many vehicles including Toyota RAV [87].

- **BTMS with parallel or series flow:** when it comes to air-based BTMSs, their flow is either parallel or series. In series-flow BTMSs, every battery module finds the same amount of air. On the other hand, the air flow is divided almost equally between the modules in parallel flow BTMSs [72], leading to a more uniform temperature distribution within the battery pack [56].

2.2.2 BTMS Design

As suggested by Pesaran [74], there are several steps in designing a BTMS: first the BTMS requirements, such as the operating climate, safety, and the available space in the vehicle, should be considered. Next, the driving scenarios, to which the vehicle may be exposed, are identified, and the associated load current and heat generation are calculated. Using the heat generation value, the thermal model can give the resulting battery temperature. Based on the observed thermal behaviour, the designer can roughly choose an initial BTMS for the system. This initial design can be further analysed and validated using more advanced analysis methods such as finite element analysis (FEA). It is then optimized, in as many

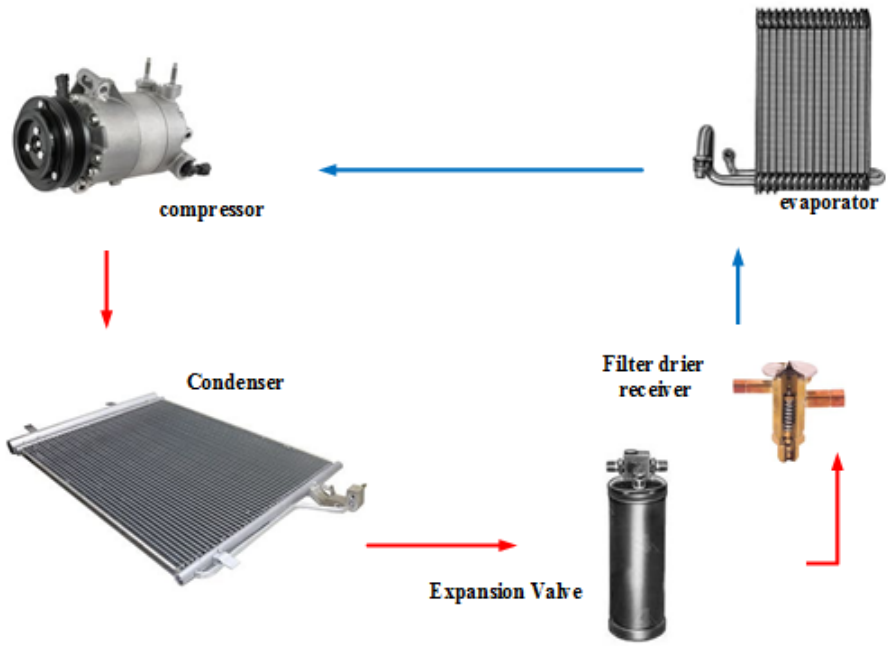

Figure 2.7: Typical refrigeration cycle in hybrid vehicles.

trials as necessary, to meet the objectives.[2]

As an example, through such a design procedure, Chen [33] examines an indirect liquid-based cooling system over both a fin-based air-cooling system for a pouch Li-ion pack under certain condition, and investigates the advantages and disadvantage of each of the methods, in terms of the temperature rise, weight, and the power cost.

Using such reasoning can demonstrate insightful results: for example, that active air-based systems are not proper for aggressive driving cycles as they cause non-uniformity in the temperature distribution [33], or the evolution of EVs, to become applicable in cold climates in addition to that of California which was where EVs were first born [72]. These examples illustrate how a factor such as climate could change the destiny of a certain design. For more or less the same reason, HEVs' design was switched, to be cooled down with the cabin air rather than the ambient [72].

[2]For further details please see [74]

2.2.3 BTMS Control-oriented Modelling

In their hearts, model-based BTMS controllers have so-called control-oriented models which are simple and real-time implementable, and include a battery model as well as a model of the actuation mechanism. In the previous section, different types of battery thermal models were explored. Here come several methods to model the actuation circuits.

The BTMS circuit control-oriented model can be considered as a constant affecting the total power drawn from the energy sources for battery tempering [20]. In fact, given the solution of the power management problem for an electrified platform, the electric power assigned to each actuator is identified. The actuators' efficiency determines how much of this power is transferred to the battery pack. Another modelling approach is merely considering the flow-rate of the BTMS circuit as it already exists in the battery heat transfer equation. In actuators such as fans, there are maps relating the flow rate to their power consumption. Circuit itself could be modelled by simple methods, such as using AMESim, where the unnecessary details are neglected [90]. One could consider a more complex control-oriented model of the BTMS circuit, with all of the components, and writes the equations based on the variables that are available for measurement through sensors; afterwards, the number of unknowns and parameters could be decreased based on the constraints in the circuit. Such an approach has not been applied in the BTMS control design context though, probably as it makes the design complicated.

2.3 Battery Thermal Management Control Problem

As stated in the previous section, the literature has proposed different approaches to address the challenging problem of BTMS design; however, there are very few examples including a control methodology.

Among those examples lies an EV BTMS controller developed by Bauer [20], where PMP is applied for the offline optimization of battery life expectancy and energy usage. This design successfully maintains the battery temperature at the desired reference point. As for another example of optimal control applications, Tao [91] suggests a BTMS controller for HEVs based on stabilizing the battery core temperature. He implements this idea using a linear optimal controller and a nonlinear back-stepping controller, and reports improvements in terms of the power conservation and reference tracking. Moreover, Tao [90] designs a BTMS controller for HEVs based on feedback optimal-control. This controller tracks the battery-core reference temperature while significantly reducing the power consumption. Further, Masoudi et al [65] demonstrates the applicability of a Dynamic

Programming based optimal controller in BTMS of EVs, where the desirable temperature is tracked and the power consumption is observed to be less than that of a benchmark PID. Rule-based controllers have been also deployed in BTMS applications, as done by Pham [75], for energy management of heavy duty hybrid electric trucks. Their strategy improves the fuel economy while taking into account the battery life. It is observed that BTMS can be implemented by means of more practical control approaches as well: Shin [83], [55] develops a real-time BTMS for EVs by regulating the physical battery-variables, where the simulation results show salient performance improvements.

2.4 Model Predictive Control

As mentioned before, the gap in the literature motivated us to formulate the BTMS controller using MPC. MPC is an online model-based strategy; at each time step, it predicts the system's evolution over a finite horizon in order to find the optimal control laws that minimize a cost function comprising the desired future behaviour of the system. In the meantime, the system model, along with the devised cost function and physical constraints, determines the computational cost and the theoretical features of the controller such as stability. Thus, the model should suggest enough details without being over complicated [21]. MPC was first legitimately introduced in the late 80s for chemical process industry applications. Nonetheless, the research in this regard can be traced back to the earlier decades. The motivation behind introducing MPC at that point was mainly addressing the existing constraint handling issues [66]; although constrained optimization suggested by MPC was not an innovation, it constituted one of the first real-time applications of large-scale dynamic optimization in the process control context [39].

So far MPC has been used for various mechanisms in the chemical process industries, from a hydrocracker reactor to distillation columns [39]. MPC, nevertheless, is not limited to the process control; Its significant advantages have cleared its path towards vast applications in other areas such as those in the automotive industry; MPC finds a near optimal solution of the problem given the model is accurate enough [21]. Being a real-time approach, MPC is fascinating to the automotive industry by itself; however, it is flexible to be improved further, in that different techniques have been applied making MPC even faster; for example, the online active set strategy suggested by Ferreau [37] provides sampling times in the order of milliseconds. Also, Falcone [35] achieves two different computational complexities using two different MPC formulations. MPC can be used to control multiple actuators simultaneously [34]. Moreover, it can handle systems with either discrete or continuous inputs [32]. This counts as an asset in the automotive subsystems

where many of the actuators may be discrete. Also, the physical constraints on the actuator inputs can be taken care of by MPC [37], as it is very well capable of systematically handling the constraints [39] on the inputs, states, and outputs. MPC makes it possible to benefit from the future information [35], where there is the flexibility to change the amount of such information required by MPC [58].

As a result of its salient properties, some of which were mentioned above, MPC has been extensively used in the automotive-related topics: MPC can address problems such as the adaptive cruise control (ACC) [68] or stabilization and yaw-rate control [34]. Autonomous driving is another front-line topic investigated through MPC [35] [29]. Moreover, there are several examples of model predictive controllers being applied as the supervisory controller for sake of the power management in the PHEVs [64] [97] [26] [27]. Specifically, the latter examples provide important insight towards BTMS MPC-based control design, as BTMS control methodology is conceptually very much similar to that of the powertrain control.

2.5 Hardware-in-the-loop Test Benches

Electronic Control Units (ECUs) are prevalently exploited in different vehicle-subsystems. Vehicle ECUs specialize in various tasks such as engine control, powertrain control, transmission control, suspension control, and so on. Testing ECUs on the actual plants dictates validation cost and time to the manufacturers [93]; therefore, accurate yet cost effective test benches are essential. HIL simulation provides a test bench that could be used for rapid prototyping at the development stage of ECUs [36], before the real-time control implementation [30]. In the meantime, HIL facilitates controller evaluation in real-time [18].

In this thesis, HIL experiments are used for further controller evaluation. It will be discussed that which ECUs are in charge of the battery thermal management in the baseline vehicles.

2.6 Summary

We provided a background on the BTMS and relevant areas, including the existing models and methods. It was observed that the research applying a feedback control thermal management mechanism is limited; Rule-based controllers were implemented, but they come with shortcomings that we have already discussed. PMP and DP were applied which

are not real-time. Also, the few suggested real time methods are based on simplifications that can be improved further.

Motivated by the above-mentioned ideas and concerned by the existing drawbacks, this study designs BTMS controllers for given electrified vehicles, namely the Toyota Prius and Toyota RAV4, using a real-time optimization method. MPC, with its discussed significant features, forms the basis of these controllers.

Chapter 3

Model Development for Baseline Platforms

This chapter introduces the BTMS structure and model components, including the energy storage system (ESS) and longitudinal dynamics, for the baseline PHEV and EV platforms.

3.1 PHEV

This section is designed as follows: first an overview of the BTMS structure in PHEV is provided. Next, the Autonomie ESS model is investigated, as Pesaran [73] suggests. Due to the shortcomings in terms of the thermal behaviour, this model is then modified. Afterwards, the system longitudinal dynamics and electrical model are introduced respectively. Finally, the control-oriented modelling procedure is explained, followed by a brief summary of the whole section.

3.1.1 BTMS Architecture

Lithium-ion batteries perform best in a certain temperature range [73], and BTMSs are designed to maintain the battery temperature within that range. To do so, different tempering strategies can be applied, as previously explained in the introduction chapter.

The vehicle in this case study has an air-based battery-cooling system, where there exist two fans providing the battery with the compartment air to cool it down. The fans are

activated by the Electronic Control Unit (ECU) commands once the temperature exceeds some desirable level, namely the reference temperature, which is obtained by the system operating condition. The rules governing the ECU in this regard can be replaced by other control strategies.

Figure 3.1: Fan vent location. Air is sucked into the battery pack through two vents in the passenger compartment.

3.1.2 ESS Autonomie Model

Having an accurate model of the ESS thermal behaviour is the key factor in designing a sound BTMS controller, as many of the ESS thermal and electrical parameters, including electrical resistance and capacity, are affected by the temperature. Here, the Simulink-based Autonomie model of the Toyota Plug-in Prius is considered, which is also offered by [73] with some modifications. The so-called external inputs to this model are the current load and compartment temperature, and the air-flow rate of the cooling fan is the control input. The output is the battery temperature.

The mathematical model of the battery lies on the following assumptions:

Assumption 1 *Battery module is considered as a lumped mass.*

Assumption 2 *The radiation heat transfer is neglected.*

Assumption 3 *The heat transfer to the battery module is a combination of conduction and convection, which is represented by a thermal resistance denoted by* R_{th}.

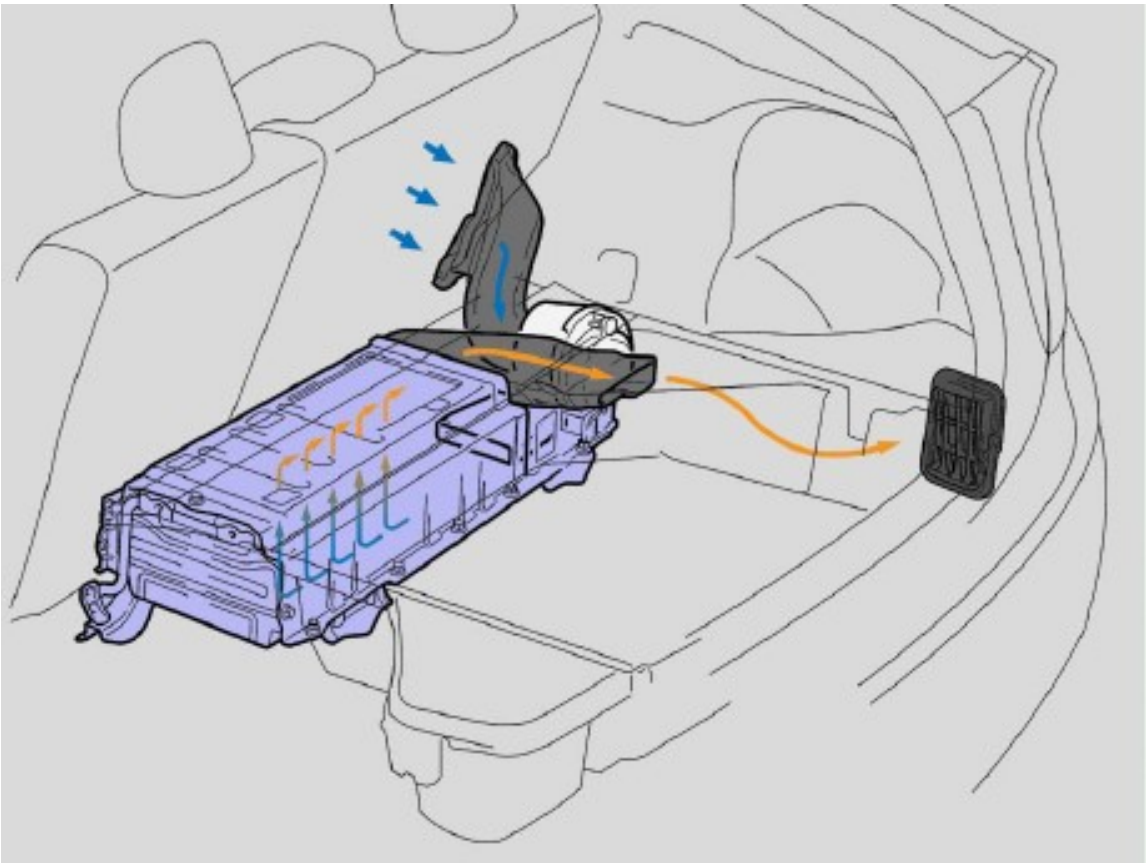

Figure 3.2: Air-flow path through the battery pack. Passenger-compartment air is applied for cooling the battery.

Assumption 4 *The only heat generation form is the Joule heating caused by the battery internal resistance.*

The thermal management mechanism works as follows: once the battery temperature exceeds the reference point, the actuator, which in this case is an on-off cooling fan, provides a constant air-flow rate, and the heat transfer between the compartment air entering the battery area and the air around the battery module is half of the heat transfer between the battery module and its surrounding air.

Using Assumptions 1 to 3, the heat transfer equation for the battery module can be formulated as

$$Q_{tf} = (T - T_{air})/R_{th}, \tag{3.1}$$

where Q_{tf} is the heat transfer, and T and T_{air} represent the temperature of the battery module and that of its surrounding air, respectively. Meanwhile, Assumption 1 can be written as

$$Q_{tf} = 2(T_{air} - T_{in})/(\dot{m}_{air} C_{p,air}). \tag{3.2}$$

Here T_{in}, $\dot{m}$, and C_p stand for the compartment-air temperature, the air-flow rate, and the heat capacity of the air, respectively.

Using Assumption 3, the rate of change in the battery temperature can be written as

$$\dot{T} = \frac{R_{bat} I_{bat}^2 - Q_{bat}}{m_{bat} C_{p,bat}} \tag{3.3}$$

Combining Equations 3.1, 3.2, and 3.3, and rewriting in a discrete fashion gives

$$\begin{aligned} T(k+1) = T(k)[1 - \frac{\Delta t}{(\frac{\dot{m}C_p}{2} + R_{th}) m_{bat} C_{p,bat}}] \\ + \frac{\Delta t}{m_{bat} C_{p,bat}} [R_{bat} I_{bat}^2 + \frac{T_{in}}{(\frac{\dot{m}C_p}{2} + R_{th})}], \end{aligned} \tag{3.4}$$

where Δt is the sampling time. Setting $\alpha = \frac{\Delta t}{m_{bat} C_{p,bat}}$ and $\beta = \frac{1}{\frac{\dot{m}C_p}{2} + R_{th}}$, Equation 3.2 can be simplified to

$$T(k+1) = T(k)(1 - \alpha\beta(\dot{m})) + \alpha(R_{bat} I_{bat}^2 + T_{in}\beta(\dot{m})). \tag{3.5}$$

Equation 3.5 demonstrates a special case where fans are on.

Assuming that below the reference point the surrounding-air temperature is equal to the compartment-air temperature, the general expression for the battery temperature can be written as the following piece-wise function:

$$T(k+1) = \begin{cases} T(k)(1 - \frac{\alpha}{R_{th}}) + & T(k) < 35 \\ \alpha(R_{bat} I_{bat}^2 + \frac{T_{in}}{R_{th}}) & \\ & \\ T(k)(1 - \alpha\beta(\dot{m})) + & 35 \leq T(k). \\ \alpha(R_{bat} I_{bat}^2 + T_{in}\beta(\dot{m})) & \end{cases} \tag{3.6}$$

Shortcomings of the Autonomie-based ESS Model

Figure 3.3 shows the Simulink-based thermal subsystem of the ESS Autonomie-model. This model is implemented based on equation 3.3. Heat generation is an input to the subsystem; it is added to the heat transfer to give the battery-temperature change-rate. Moreover, the heat transfer is calculated in a separate subsystem, as demonstrated in Figure 3.4.

As the main-ESS inputs, the ambient temperature and air-flow rate are identified by two constant blocks which can be replaced by other blocks or subsystems of interest in order to modify the model. The current load, although not shown, is used to calculate the heat generation.

Although [73] maintains that the effective thermal resistance is a piece-wise function of the air-flow rate, such an approach is not followed in Autonomie. This can also be seen in Figure 3.4, where the constant block representing R_{th} accepts two values: one for the situations when the fan is on, and the other one for when it is off. This makes sense only when the air-flow rate equals the default value offered by Autonomie; thus, R_{th} block should be modified and replaced by a user-defined function of the air-flow rate to represent a general case before we can change the value of the air-flow rate or the fan type.

Another shortcoming worth mentioning is that the rule-based controller applied in the Autonomie software activates when temperature reaches 35 °C; however, there exist other studies suggesting other rule-based scenarios. For example, Zolot [101] states that the Prius fans turn on at 35 °C and continue working till the temperature decreases to 33 °C.

3.1.3 Modified ESS Model

The ESS model provided by the Autonomie software is simple yet suited to real-time control purposes. Nevertheless, this model has limitations that can totally disqualify it in certain applications: it only models the heat transfer in rule-based BTMSs with an on-off fan, whereas other control strategies may necessitate the use of continuous air flow values. Moreover, the fan size may not be proper for particular situations. Specifically, the default fan used in the Autonmoie model cannot cover all of the trip scenarios that the vehicle may be exposed to, as will be shown later. As a result, a more general ESS model capable of representing the cases where the actuator happens to be different, such as a multi-stage or continuous fan, or even an on-off fan of a bigger size, has to be considered. Here the model offered by Yuksel [99] is applied, with minor modifications.

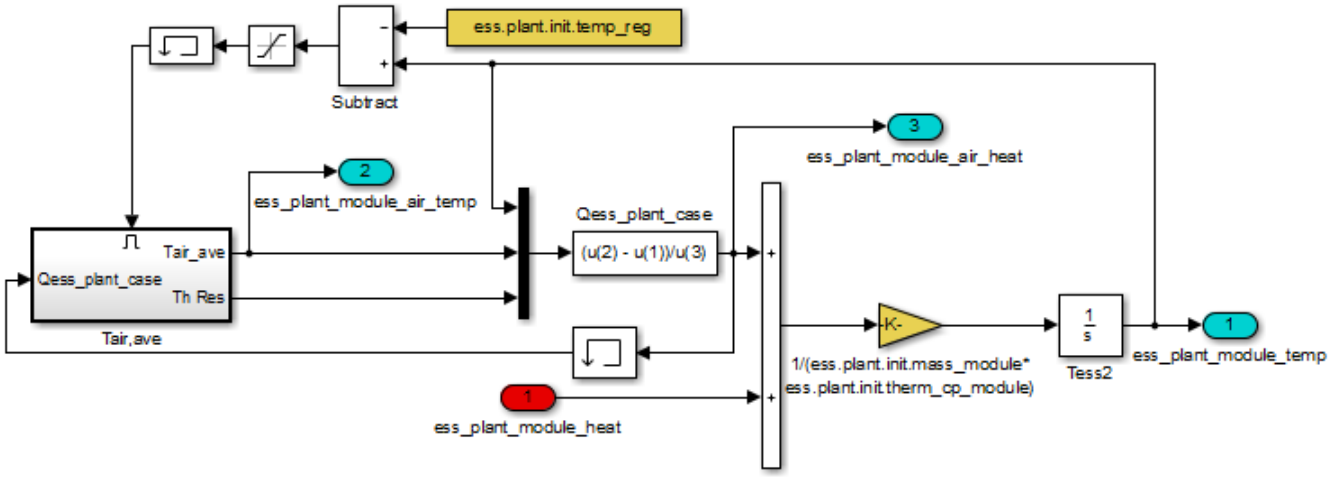

Figure 3.3: Temperature calculation subsystem.

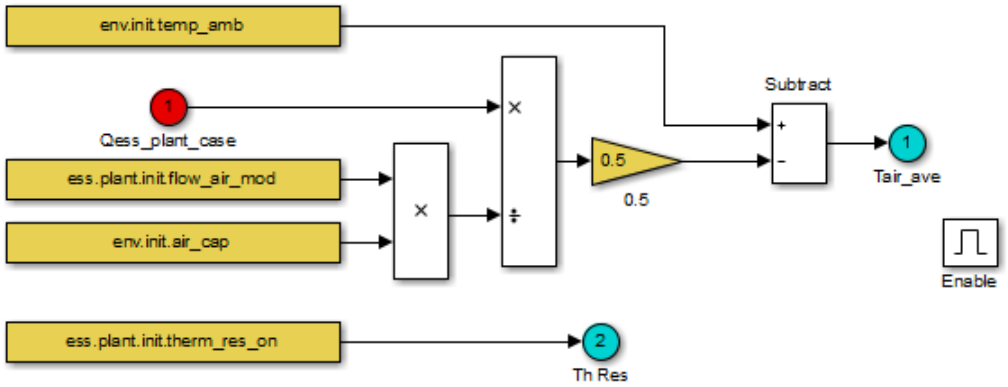

Figure 3.4: Heat transfer calculation subsystem. R_{th} and air-flow rate modelled by constant blocks.

This new model is fundamentally different from the previous one, mainly in that its input is air velocity rather than the air flow rate. It will be observed later that this is not an issue, as the air velocity and flow rate in a fan can be mapped to one another using the duct geometry.

The PHEV in this case-study is a Toyota Plug-in Prius with a passive cooling system and parallel flow; therefore, only one module is modelled and simulated, and the results are extended to the whole battery pack.

Due to the first law of thermodynamics and given the battery module as a control volume, any change in module temperature can be because of either the heat generation or the heat being transferred to the pack through the control volume boundaries. The equation can be shown as

$$\dot{T} = \frac{\dot{Q}_{gen} - \dot{Q}_{tf}}{m_{bat} C_{p,bat}}, \tag{3.7}$$

where $\dot{Q}_{gen}$ and $\dot{Q}_{tf}$ are the rates of the heat generation and heat transfer respectively, and m_{bat} and $C_{p,bat}$ stand for module mass and thermal capacity.

Now $\dot{Q}_{gen}$ and $\dot{Q}_{tf}$ should be calculated. Here the only form of the heat generation considered is Joule heating. As a result of the parallel flow, all of the cells in a module are assumed to carry the same current; therefore, the module heat-generation becomes

$$\dot{Q}_{gen} = N R_{bat} I_{bat}^2, \tag{3.8}$$

with N being the number of cells per module and I_{bat} being the cell current.

There are different ways to model the heat transfer to the battery module based on the coolant passing across it. Without loss of generality, cells can be approximately assumed to have a staggered layout [99]. This assumption enables us to write the heat transfer as

$$\dot{Q_{tf}} = N \pi h d \Delta T L, \tag{3.9}$$

where d is the cell diameter, L is the cell length, and ΔT is the log mean temperature difference defined as

$$\Delta T = \frac{(T - T_{in}) - (T - T_{out})}{\ln(\frac{(T - T_{in})}{(T - T_{out})})}. \tag{3.10}$$

The final step in calculating $\dot{Q_{tf}}$ will be finding an expression for h, the heat transfer coefficient. It can be obtained using

$$h = \frac{Nuk}{d}, \tag{3.11}$$

where k is air thermal conductivity and Nu is the Nusselt number. Nu can be found using

$$Nu = C Re_{max}^m Pr^{0.36} (\frac{Pr}{Pr_s})^{1/4}. \tag{3.12}$$

Pr is the Prandtl number, and Re_{max} is the Reynolds number at maximum air velocity, both of which calculated at the film temperature,

$$T_f = (T + T_{in})/2. \tag{3.13}$$

C and m are constants evaluated at Re_{max}, as shown in Table 3.2. Here, it has been assumed that the maximum velocity is equal to the average velocity provided by the controller, or in other words, the effect of velocity profile is neglected.

Reynolds number is defined as follows:

$$Re = \frac{Vd}{\nu}, \tag{3.14}$$

where ν is the kinematic viscosity, a function of the air temperature.

To find the outlet air temperature, T_{out}, one can use the fact that the heat transfer between the cell surface and the air, calculated using Equation 3.9, causes an increase in the air temperature. In other words,

$$\frac{T - T_{out}}{T - T_{in}} = \exp\left(-\frac{N\pi hd}{\rho_{air} V_{air} N_T S_T C_{air}}\right). \tag{3.15}$$

Here S_T is the transverse pitch, N_T is the cell number in transverse direction, and C_{air} is the air specific heat.

Table 3.1 shows the numeric value of the geometric constants in the battery model. The values for the outlet temperature are also available in a map-based format [78].

Table 3.1: Battery Pack Dimensions

Cell Size	d	S_T	L	N	N_T
L-AA	50	837	970	3	25

3.1.4 Simulink Implementation of the Modified ESS Model

Comparison between the concept of the modified model with that of the Autonomie shows that the new model can be implemented by modifying the Autonomie ESS model, because the only part that should be updated is the heat transfer calculation block, along with its activation strategy. Once updated, this block can reflect the desired thermal behaviour in

Table 3.2: Constants of Equation 3.12 for Staggered Flow [23]

Reynolds	C	m
$10 - 10^2$	0.90	0.40
$10^2 - 10^3$		Isolated cylinder approximation
$10^3 - 2 \times 10^5$	0.40	0.60
$2 \times 10^5 - 2 \times 10^6$	0.022	0.84

a more general manner. To provide more details, we first explain the procedure of developing the heat transfer block. Then, we modify this block further to facilitate switching between the cases with and without thermal management. Finally, the model is tested and simulation results are demonstrated.

Heat Transfer Block Implementation

The Simulink design can be modified such that the input to this system is the air velocity rather than the air-flow rate. This design can be used when the constant air velocity is applied throughout the whole simulation, or in other words the fan is always on. Figure 3.5 shows the subsystem in charge of calculating the heat transfer in this case. The first step in developing such a system is to include the required non-constant parameters in the Simulink. Based on Equation 3.9, the heat transfer term has two non-constant terms: h and ΔT, also calculated within two separate subsystems (as demonstrated in Figures 3.6 and 3.7 respectively).

Due to Equation 3.11, h is a function of the Nusselt number (Equation 3.12), and therefore C, m, Re, Pr, and Pr_s are required. Assuming the air as an ideal gas, Prandtl number is a function of the temperature; thus, Pr and Pr_s can be modelled as temperature maps. Pr_s is read at the battery-surface temperature which is provided by the battery-temperature feedback. Pr, however, is read at the film temperature. Air thermal conductivity should also be read at the film temperature.

The maximum Reynolds number is calculated using the maximum velocity. The maximum velocity is geometry-wise and depends on how the battery-pack is exposed to the maximum flow rate. It is calculated using the following equation [23]

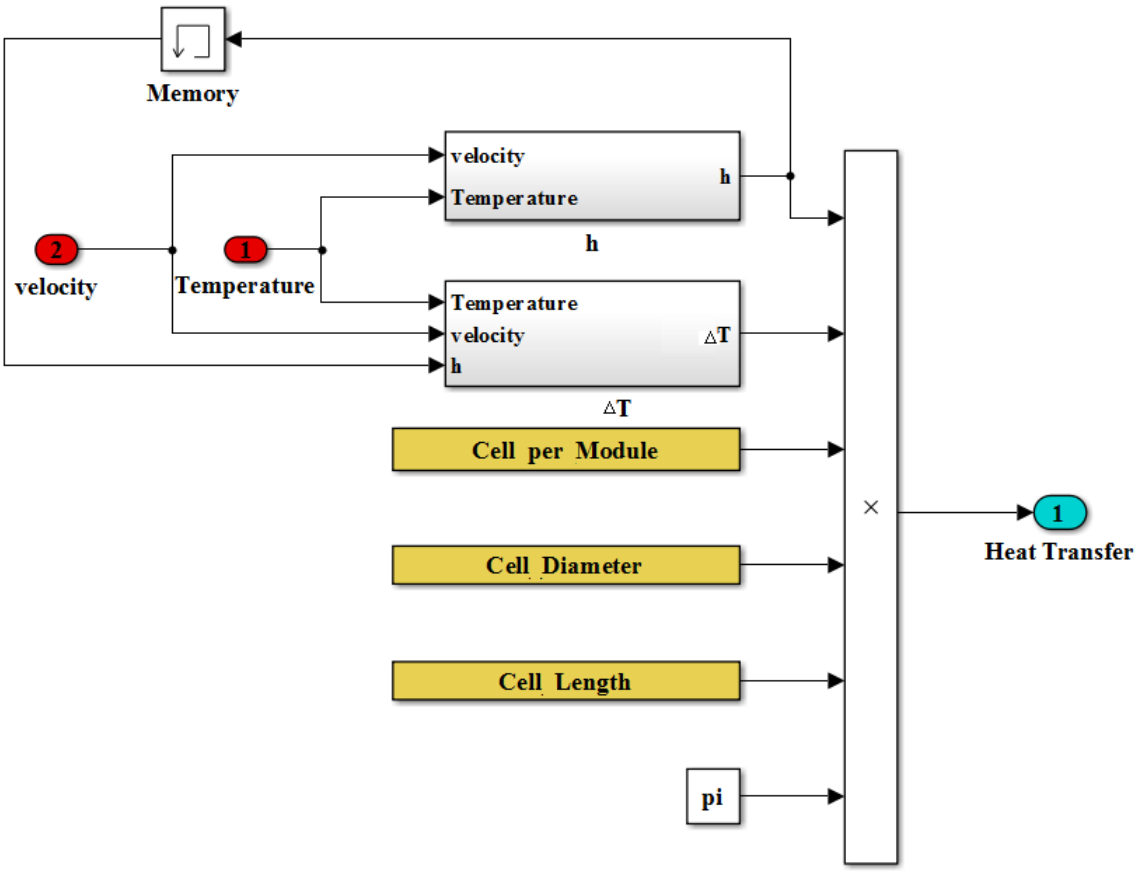

Figure 3.5: Heat transfer calculation subsystem in the modified model.

$$V_{max} = \begin{cases} \dfrac{S_T}{S_T - D} & 2(S_D - D) < (S_T - D) \\ \dfrac{S_T}{2(S_D - D)} & 2(S_D - D) > (S_T - D) \end{cases} \tag{3.16}$$

or

$$V_{max} = \frac{S_T}{max[(S_T - D), 2(S_D - D)]}. \tag{3.17}$$

In the considered geometry, it can be observed that $2(S_D - D) < (S_T - D)$. Based on

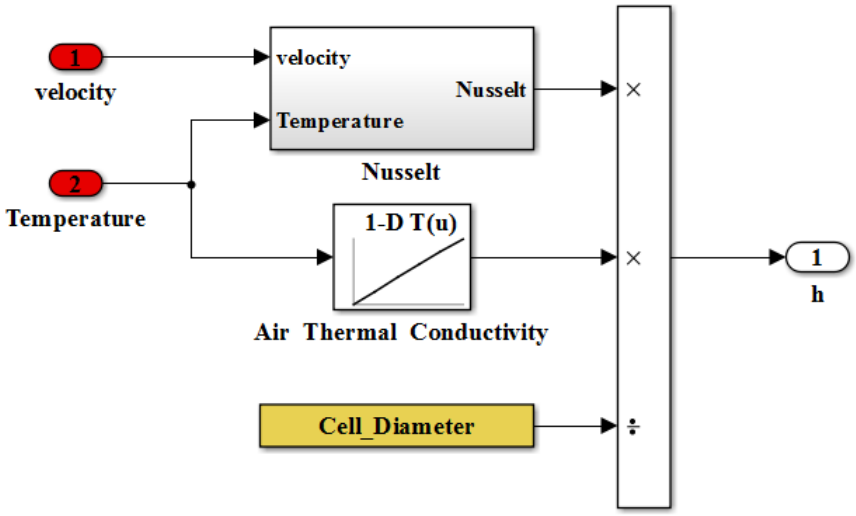

Figure 3.6: h calculation subsystem in the modified model.

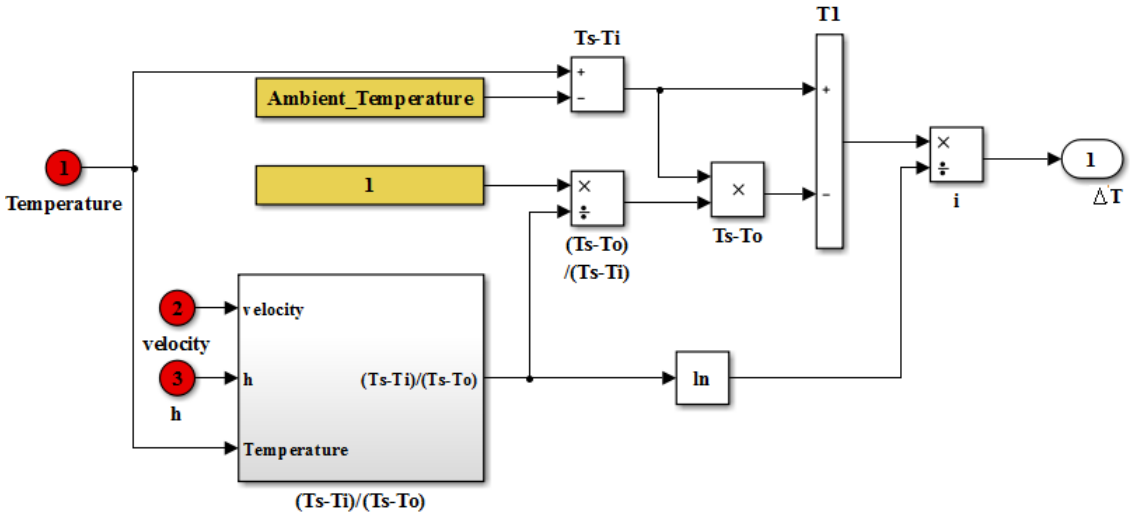

Figure 3.7: ΔT calculation subsystem in the modified model.

this, the maximum velocity is calculated by adding a gain to the velocity input. Assuming $S_T = 1.4d$, this gain is equal to 3.5.

The next step is regarding the calculation of C and m; as they are functions of the Reynolds number, they can be found using a one-dimensional look-up table block.

To find ΔT, there should also be a sub-system in charge of calculating $\frac{(T_s - T_i)}{T_s - T_o}$ using Equation 3.15. The geometrical constants used in this equation are available in Table 3.1. The non-constant parameters, including C_p and ρ , should be considered as maps. Finally, $\bar{h}$ is fed back into this sub-system once calculated in its own subsystem.

All of the maps that are considered in the modified Simulink model are shown in Table 3.3. These maps are prepared based on the online information [7].

Table 3.3: Maps in the modified Simulink model [7]

T	T_f	ν	Pr_s	Pr	ρ	C_p	k
°C	°C	$\times 10^{-5}\, m^2/s$	–	–	kg/m^3	$\times 10^3 J/kg°C$	$W/m°C$
0	10	1.421	0.7198	0.7176	1.247	1.006	0.02484
10	15	1.466	0.7176	0.7166	1.226	1.006	0.02522
20	20	1.511	0.7156	0.7156	1.205	1.006	0.02560
30	25	1.557	0.7138	0.7147	1.185	1.006	0.02600
40	30	1.604	0.7121	0.7138	1.165	1.007	0.02634
50	35	1.651	0.7105	0.7129	1.146	1.007	0.02671

Aside on the High-fidelity Model's Velocity Approximation

Inside the model structure, a parameter called k is assumed to tune the air velocity value. As the only available valid data to do so is that obtained by Autonomie, the goal here is to identify what air velocity range results in a similar temperature profile as the one obtained by Autonomie.

The simulations in this regard could be done over the same cycles (or in fact the same load current) and with the assumption that in both of the cases the fan is on all the time. In Figure 3.8, it is illustrated that how changing k could affect the temperature. The best accordance with the Autonomie behaviour is observed when $k = 13$. When $k = 1$, the temperature goes highly further compared to the time when k is increased to the order of 10; thus, the high importance of BTMS is observed, even in such a short driving cycle.

One may argue that as this tuning has been done over a certain cycle (UDDS), there is always the chance that such k does not work in other cases; however, calculations below show that how such k value makes sense.

In Autonomie, we have the air-flow rate as $\dot{m} = 0.0058\frac{kg}{s}$. As the average density

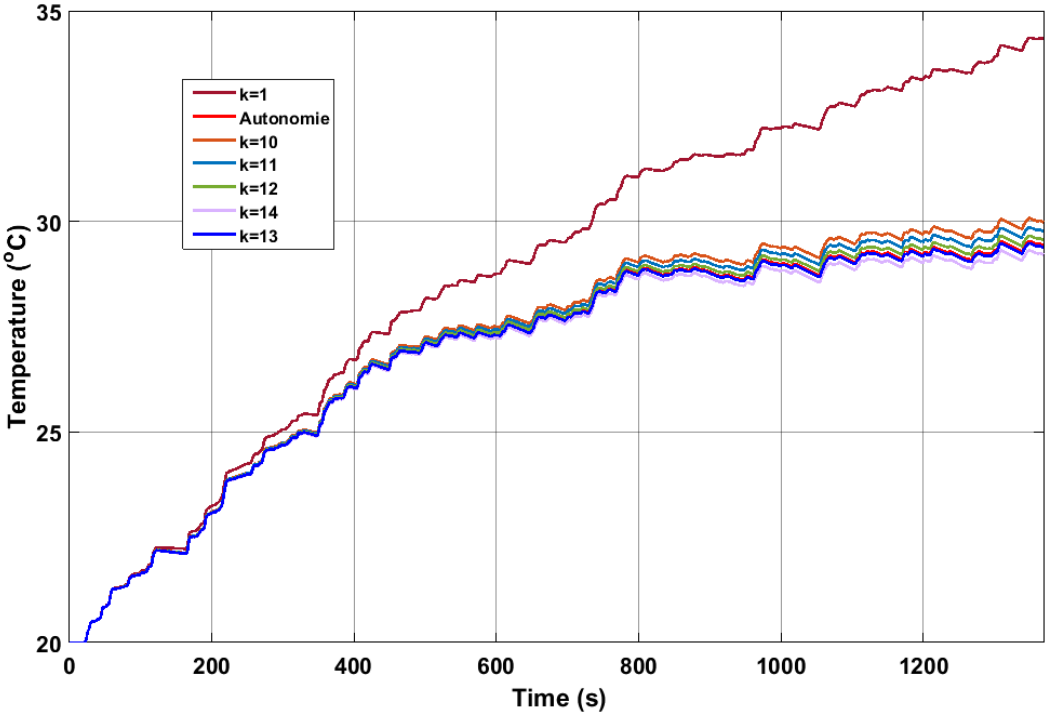

Figure 3.8: Air-flow rate impact on temperature. Fan on all the time.

(average of the data in Table 3.3) is equal to $\bar{\rho} = 1.1955\frac{kg}{m^3}$, we could write the volumetric flow-rate, or Q, as

$$Q = \frac{\dot{m}}{\bar{\rho}} \approx 0.0048\frac{m^3}{s} = VA, \tag{3.18}$$

where A is the fan-duct area and V is the velocity. From here, using the value $V = 13 \times 1.83 \approx 24$, we get $A = \frac{Q}{V} = 2cm^2$, which becomes $2cm^2 * 25 = 50cm^2$ for the whole pack. This value can be compared with the actual duct area of the Prius-fan: the Prius fan in the Green and Intelligent Automotive (GAIA) research facility was disassembled, and its duct-area was measured to be $4.5 * 5.5 = 24.75cm^2$. As there are two of them in a battery pack, the duct area for the whole pack becomes $50cm^2$; therefore, the two values match. The maximum velocity associated with the existing fan can be considered equal to $24\frac{m}{s}$ over the course of this research. This would be also the input upper limit as of an inequality constraint.

Switching Scenarios

As opposed to the Simulink Structures in Figures 3.3 and 3.4, where the fan is activated when temperature exceeds the regulation temperature, the new architecture should be modified further to facilitate shifting between two cases, namely with and without thermal management. To switch back and forth between the conditions where there is and there is not forced convection, the new high-fidelity model is modified such that there exists an if block such that if the fan velocity, defined by the controller, is equal to zero, the modified Simulink model is activated; otherwise, the Autonomie model for natural convection is applied. The schematic Simulink diagram of such a layout is shown in Figure 3.9. This is also the final model considered in the MIL and HIL simulations in Chapter 5. Figure 3.10 shows the results of this block for a random air-velocity profile to demonstrate how it actually works. In cases with zero velocity and non-zero velocity, different heat transfer blocks are activated.

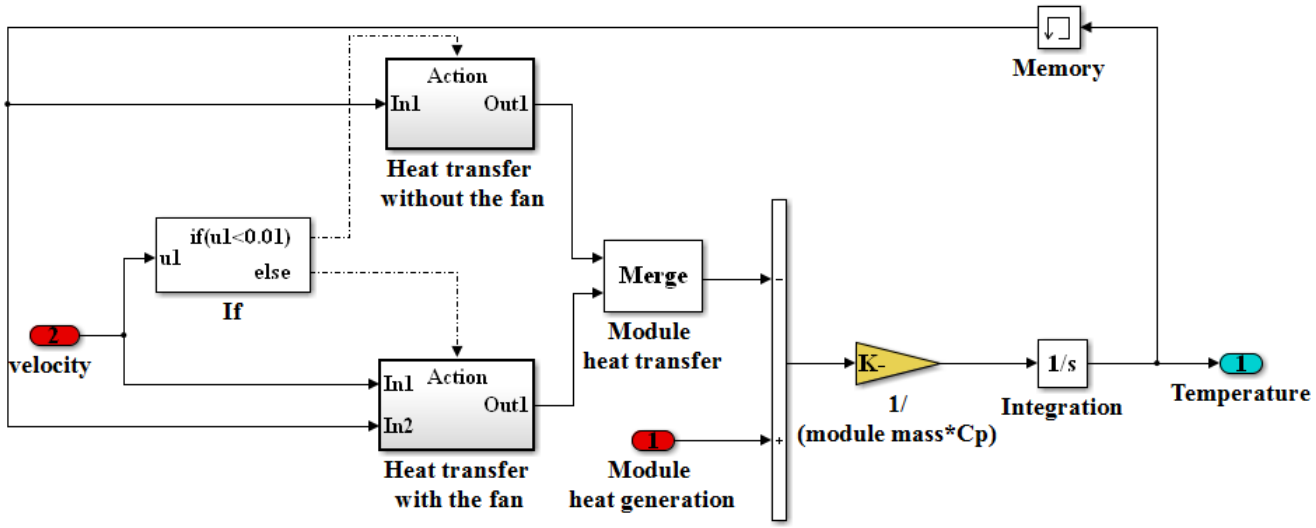

Figure 3.9: High-fidelity model with actuation temperature and if statement (switch).

3.1.5 ESS Control-oriented Modeling

Although the high-fidelity model represents system behaviour accurately, it is not meant to be applied for a real-time BTMS controller. A simplified, namely control-oriented, model facilitates real-time simulations while providing an acceptable accuracy. Such a model

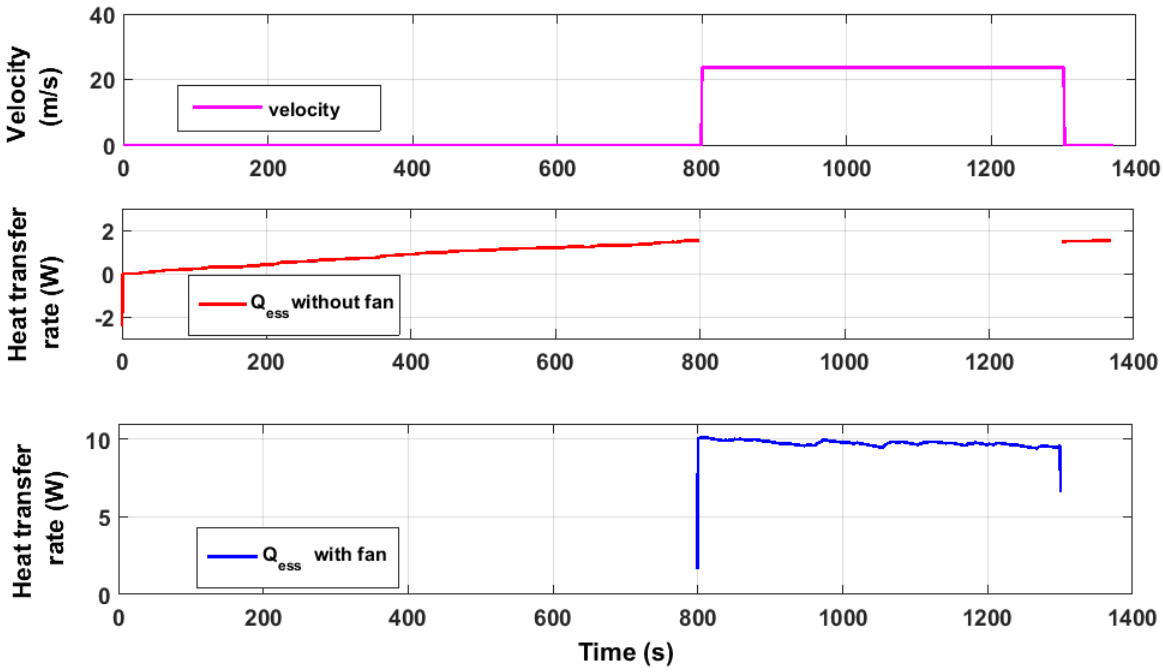

Figure 3.10: High-fidelity model test. Results over UDDS cycle for a random fan-velocity profile.

can be based on the same previous equations, with considering some of the parameters constant.

The initial step of control-oriented modelling could be considering the values obtained by taking the average of the maps in Table 3.3; Table 3.4 shows such constant parameters. Figure 3.11 shows the performance of this control-oriented model with respect to the high-fidelity model. Even though this performance seems acceptable, the applied control-oriented model can be cross-validated using the the high-fidelity model to make the controller design even more accurate. The parameter identification procedure in this regard is explained in the following.

Table 3.4: Constant parameters of the control-oriented model.

Parameter	Value
Pr	0.715
Pr_s	0.715
Re	2.21×10^4
ν	$1.54 \times 10^{-}5m^2/s$
ρ	$1.2kg/m^3$
k	$0.026W/m^oC$
C_p	$1009J/kg^oC$

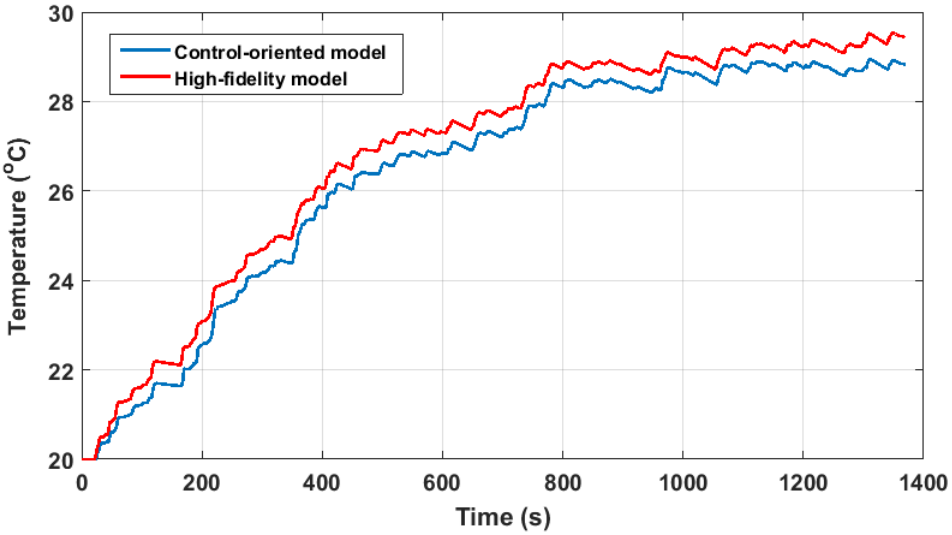

Figure 3.11: Initial control-oriented model versus high-fidelity model. Fan is on all the time.

Parameter Identification

Here, the parameter identification is done for cross-validation. Initially, six constant parameters were considered for the control-oriented model; however, it can be represented by

merely three constant parameters, namely A_1, A_2, A_3, through the following formulation:

$$T_o = T - (T - T_{amb}) \exp(\frac{A_3}{V}),$$

$$\Delta T = \frac{(T - T_{amb}) - (T - T_o)}{log((T - T_{amb})/(T - T_o))}, \tag{3.19}$$

$$\dot{T} = 3A_1 I_{bat}^2 - (A_2 V^m)\Delta T.$$

To identify these constant parameters, least square method can be applied. The associated accumulative error can be defined as

$$Error = \sum_{i=1}^{n} (T_{ref,i} - T_i)^2, \tag{3.20}$$

where T_{ref} is the valid temperature data obtained from the high-fidelity model, and n represents the number of measurements. T_i is the temperature obtained from the system dynamics at the i^{th} time step. When minimized with respect to A_1, A_2, A_3, this error gives the optimum values of the three parameters. As such, given similar inputs, namely load current, ambient temperature, and air velocity, the results of the control-oriented model follow those of the high-fidelity model with a minimum error. It should be called attention to the fact that the parameters for the initial condition of parameter identification here are those mentioned for in Table 3.4 as for first trial. fminsearch, included in Matlab optimization toolbox, was applied as for solver [9].

As the parameter identification should be valid for a variety of driving scenarios, different driving cycles were combined to provide a diverse input. The default driving cycle in the Autonomie is UDDS with a duration of 1369 seconds, comprising of a 505-seconds cold start phase and a 846-seconds transient phase. This was added to the load currents of FTP-75 cycle, as well as those of the US06, and the combination of the three of the load currents was considered as the input to the system. This was for the data to be diverse as US06 provides a combination of city and high-way driving [10]. For this input, the results found using fminsearch were as follows:

$$(A_1, A_2, A_3) = (4.65001845538083\times10^{-6},\ 204.191388712604\times10^{-6},\ -4.75823397492004\times10^{-3}). \tag{3.21}$$

Using the values of A_1, A_2, and A_3 as such results in an acceptable thermal behaviour. Figures 3.12, 5.10, and 3.14 show the results of control-oriented model compared to the

high-fidelity over FTP-75, UDDS, and US06 drive cycles respectively. The percentage of the relative errors of the considered three-parameter control-oriented model equals 0.776 % for the UDDS cycle, 1.56 % for US06, and 0.474 % for the FTP-75 drive cycle. Equation 3.22 shows how the error is calculated.

$$error(\%) = (\sum_{i=1}^{n} \frac{|T_i - T_{valid,i}|}{T_{valid,i}} \times 100)/n \tag{3.22}$$

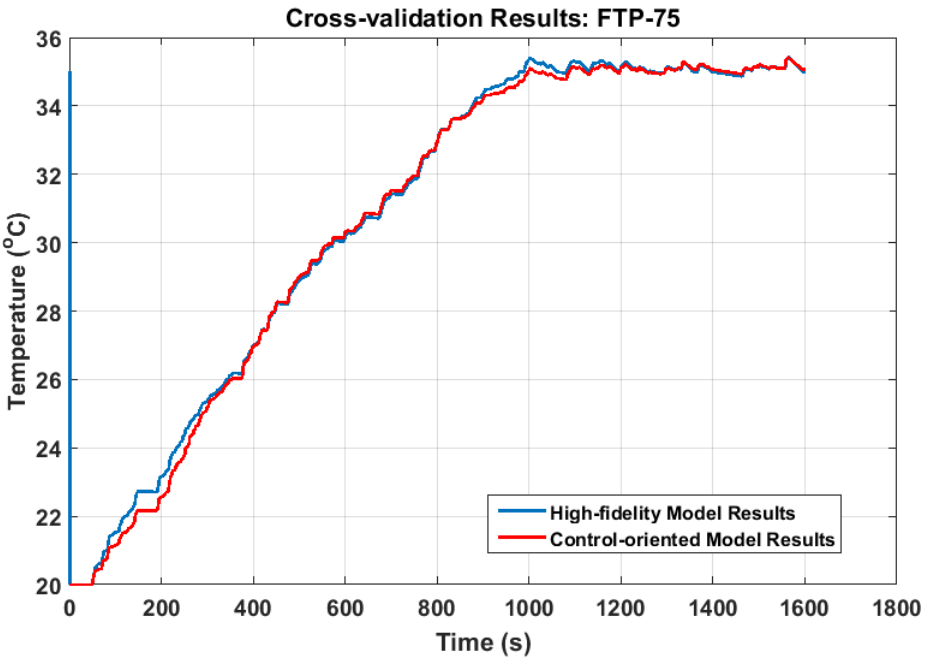

Figure 3.12: Control-oriented model versus high-fidelity model. FTP-75 driving cycle.

A second parameter identification was conducted, this time with five parameters, including two for the case when the fan is off. As it was mentioned earlier, in the cases that the fan is off, we switch to a model like Autonomie. This results in considering one constant, namely A_4, for the thermal resistance (or R_{th}, resulting form conduction and natural convection as Equation 3.1 suggested), and a second constant, A_5, for $m_{bat} \times C_{P,batt}$ as in Equation 3.3. The results of this cross-validation over FTP-75 and UDDS cycles are demonstrated in Figures 3.15 and 3.16, respectively. It is observed that adding two parameters does not significantly improve the performance so we will consider the first three parameters; this is expected as the electrical resistance along with the parameters

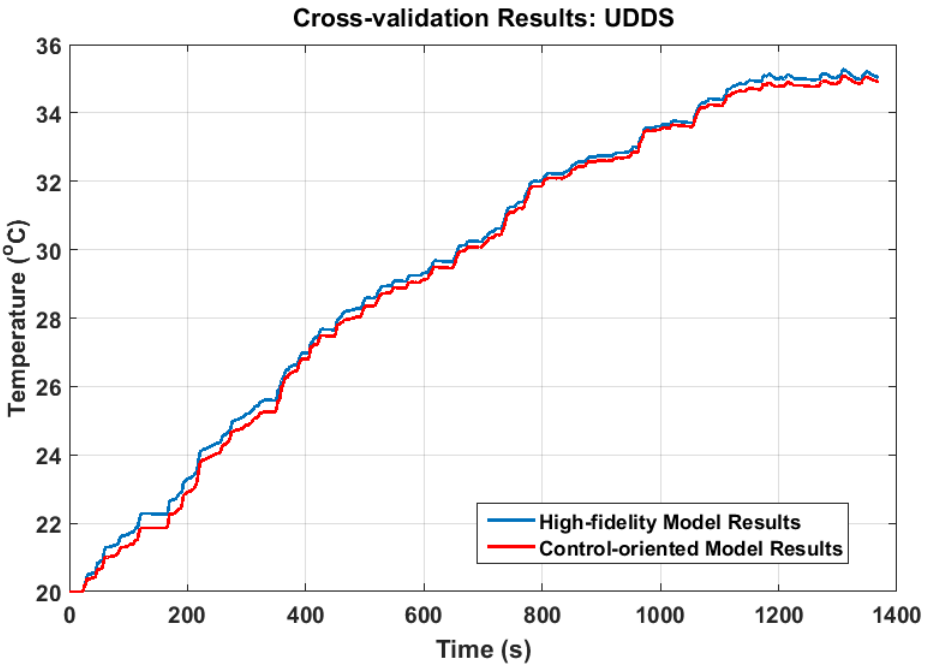

Figure 3.13: Control-oriented model versus high-fidelity model. UDDS driving cycle.

associated with convection are the most important phenomena affecting the physics of this problem.

3.1.6 Powertrain Model

As explained before, BTMS problem is formulated with the load current as an input. Discussions and results, however, are presented based on the driving cycles. This is due to the fact that the followed driving cycle could translate into the current drawn from the battery. Here Autonomie model is applied in this regard, where the model is run for every driving cycle, and the energy management problem is solved to give the load current profile. This profile is then used as the input to BTMS. A schematic of the Autonomie model and its powertrain is observed in Figure 3.17.

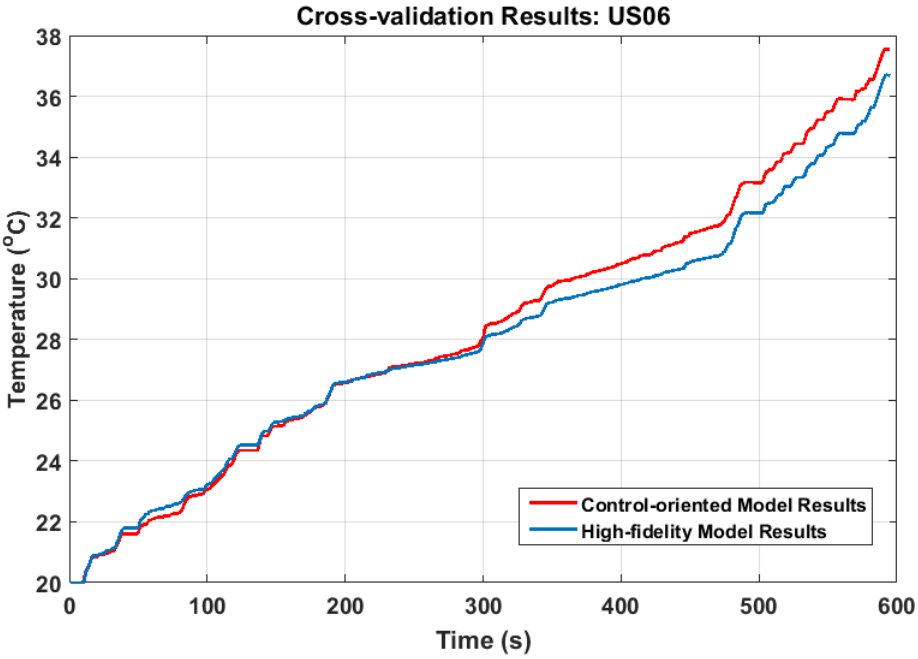

Figure 3.14: Control-oriented model versus high-fidelity model. US06 driving cycle.

3.1.7 Electrical Subsystem

As for the equivalent circuit model, Autonomie electrical subsystem is applied here, which is a Rint model (Figure 2.2) with its parameters (such as charge and discharge coefficients) being maps of temperature and SOC.

3.2 EV

This section deals with the BTMS-model components for the Toyota RAV4 EV. In this case the control-oriented and simulation models are the same as the main focus of this thesis is on PHEV. First, we introduce the BTMS in the RAV4 EV; then, we will look at the applied model which includes three sub-systems: an equivalent circuit representing the properties of battery electrical behaviour, a simplified lumped mass model introducing the thermal aspects of the battery, and a subsystem for the vehicle's longitudinal dynamics.

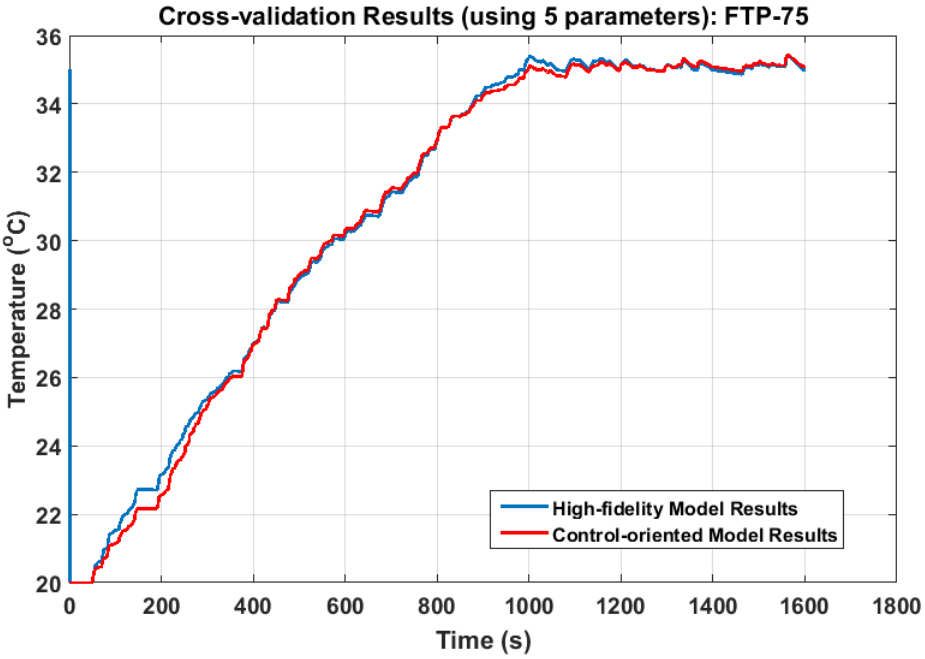

Figure 3.15: Control-oriented model with five parameters versus high-fidelity model. FTP-75 driving cycle.

3.2.1 BTMS Structure

RAV4 EV has an active thermal management system, with components such as compressor, evaporator, and so on. Here an efficiency term is applied to represent the control-oriented model of the thermal management circuit.

3.2.2 Electrical Subsystem

The battery electrical system can be simply modelled by means of a voltage source U_{OC} along with an internal resistance (R_{bat}) in series [20], or the so-called R_{int} model (Figure 2.2). The current can be calculated by

$$I_{bat} = \frac{P_{bat}}{U_{bat}}, \tag{3.23}$$

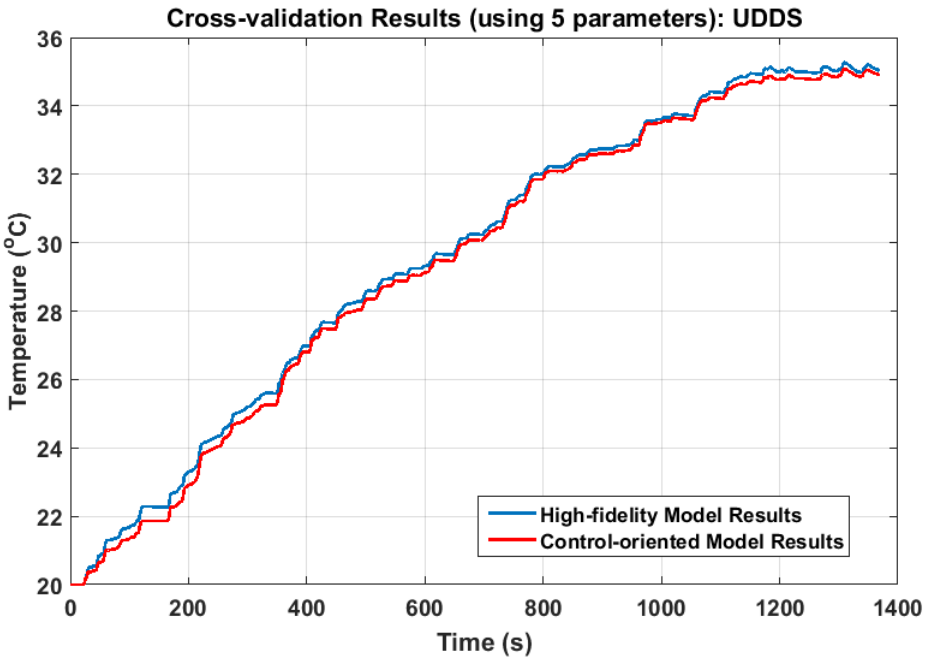

Figure 3.16: Control-oriented model with five parameters versus high-fidelity model. UDDS driving cycle.

where P_{bat} is the battery power. The terminal voltage U_{bat} can be written as

$$U_{bat} = U_{OC} - RI_{bat}. \tag{3.24}$$

Equations 3.23 and 3.24 are then combined to result in the following equation:

$$I_{bat} = \frac{U_{OC} - \sqrt{{U_{OC}}^2 - 4RP_{bat}}}{2R}. \tag{3.25}$$

In Equation 3.25, only the positive root is taken into account as the battery current increases with respect to higher power demands. To explain the relationship between the batterys SOC and the current, one can define the battery capacity such that

$$\dot{SOC} = \frac{I_{bat}}{C}. \tag{3.26}$$

As a result, Equation 3.25 can be rewritten as

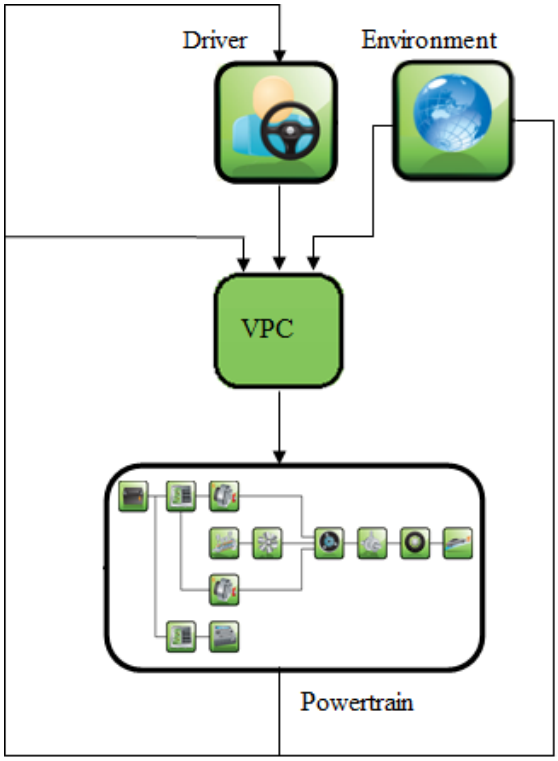

Figure 3.17: Autonomie model layout.

$$\dot{SOC} = \frac{U_{OC} - \sqrt{{U_{OC}}^2 - 4RP_{bat}}}{2RC}. \tag{3.27}$$

In reality, the battery internal resistance is affected by the temperature and SOC; however, many of the case studies in the literature (see [76] as an example) consider it as a constant value. This assumption is also made here, due to the low sensitivity of the resistance with respect to the aforementioned variables.

3.2.3 Thermal Subsystem

For modelling the thermal effects, battery is assumed to be a lumped mass with the corresponding heat capacity, C_{th}. Part of the battery power, called the heating power (P_{heat}), is consumed to have the battery temperature follow a specific trajectory [20]. This power is

then transmitted to the battery's body through some thermal paths. Thus, the heat flow rate to the battery $\dot{Q}$ can be given as

$$\dot{Q} = \begin{cases} k_1\dot{Q} & \dot{Q} \geq 0 \\ & , k_1 \\ k_2\dot{Q} & \dot{Q} \leq 0 \end{cases} \tag{3.28}$$

where k_1 and k_2 are some constants representing the efficiency of the thermal circuit. It can be observed that heat P is always positive which means that either for the cooling or the heating, some of the battery power should be consumed. The equation for the battery temperature then becomes

$$\dot{\theta} = -\frac{RI_{bat}^2 + \dot{Q}}{C_{th}} = -\frac{R(\frac{U_{OC} - \sqrt{{U_{OC}}^2 - 4RP_{bat}}}{2R})^2 + \dot{Q}}{C_{th}} \tag{3.29}$$

There always exists some heat exchange between the battery and the surrounding ambient, the most significant form of which is the conduction; however, by using a dimensional analysis, it can be concluded that this heat exchange can be neglected, as compared to $\dot{Q}$.

3.2.4 Longitudinal Dynamics

Due to the vehicle longitudinal dynamics, the power demanded for driving the vehicle should overcome three dominant forces affecting the vehicle, which are the inertia, rolling resistance and aerodynamic force; consequently, the governing equations become

$$P_{dem} = \begin{cases} (\frac{\dot{v} + F_{aero} + F_{roll}}{\eta})v & propelling \\ \\ (\dot{v} + F_{aero} + F_{roll})v\eta & braking \\ \\ \end{cases} \tag{3.30}$$

where v and m are the vehicle velocity and mass, and F_{roll} and F_{aero} stand for the rolling resistance and the aerodynamic force, respectively; moreover, η shows some sort of efficiency related to the vehicle traction system. The rolling resistance and aerodynamic force are obtained from the following equations:

$$F_{roll} = C_r mg, \tag{3.31}$$

and

$$F_{aero} = 0.5\rho A_{fr} C_d v^2. \tag{3.32}$$

In the two last equations, C_r ,A_{fr} , C_d and ρ are the rolling resistance, frontal area, drag coefficient, and air density, respectively. It can be concluded that by having the velocity and forces applied to the vehicle, one can find the demanded power through Equation 3.30.

The three above-mentioned sub-systems are related through the following equation, as the battery should supply the whole amount of the power required for both driving and tempering

$$P_{bat} = P_{dem} + P_{temp}. \tag{3.33}$$

Obviously, the demanded power obtained from the speed profile of the vehicle is added to the power in charge of heating or cooling the battery to generate the total battery power, which in turn identifies the changes in the temperature and SOC, as given in Equations 3.27 and 3.29.

Chapter 4

BTMS Control Design

This chapter explains different methods applied for controller design in this research.

MPC potentials have been explicitly discussed before; it predicts the evolution of the thermal system's behaviour. Moreover, it is capable of handling the state and input constraints that should be addressed in the thermal management problem. Thus, MPC is a promising candidate for BTMS problem. As observed in the previous sections and provided equations, thermal systems have nonlinear dynamics. Nonlinear behaviour is encountered in the very first phenomenon, namely heat generation. Nonlinearites are also evident at different stages of the developed battery model. Linearization may result in ignoring parts of the system's actual behaviour and thus poor controller performance. This motivates us to formulate the problem in a nonlinear fashion to reflect all of these issues. As such, NMPC is chosen as the main control strategy for thermal management.

The proposed NMPC controller is then benchmarked against a variety of methods, such as RB controller, DP controller, the case with the fan on all the time, and PID controller.

RB algorithm is the method currently applied for fan actuation, and therefore any new suggested controller should be compared with RB to investigate if it improves the thermal management system. No controller can be expected to outperform DP because it finds the global optimal behaviour of the system, therefore forming a baseline for the solution of any other controller. Simulations with fan on all-the time demonstrate the maximum ability of the system's existing actuator. Examining this strategy is insightful since if the results are unsatisfactory, merely updating the control rules cannot alleviate the BTMS problem, and the actuators should be upsized. PID is a very common approach in the industry. Here, it is applied to investigate what NMPC has to offer over typical methods such as PID.

To cover all of the above ideas, this chapter is designed as follows: first the mathematical background, including the formulas and hypotheses applied throughout the chapter, are introduced. Next, the general formulation of NMPC is provided, followed by the details of each of the platforms- including the devised objective functions. Finally, the benchmark methods are explained.

4.1 Mathematical Background

In this section, some of the definitions and theorems used in controller design procedure are provided.

Theorem 1 ***Linear Approximation*** [1] *Given continuously differentiable function* $F : \mathbb{R}^n \mapsto \mathbb{R}$ *and vector* $d \in \mathbb{R}^n$*, one could write*

$$F(x+d) = F(x) + \nabla F(x+td)^T d, \tag{4.1}$$

for some $t \in (0,1)$*. Here, function* F *is said to have been approximated linearly.*

Theorem 2 ***Quadratic Approximation*** [2] *If function* $F : \mathbb{R}^n \mapsto \mathbb{R}$ *is twice continuously differentiable and vector* $d \in \mathbb{R}^n$*, in addition to Equation 4.1, the following is valid for some* $t \in (0,1)$*:*

$$F(x+d) = F(x) + \nabla F(x+td)^T d + \frac{1}{2} d^T \nabla^2 F(x+td) d. \tag{4.2}$$

This is called the quadratic approximation of F*.*

Definition 1 ***Quadratic Programming Problem*** [3] *An optimization problem of the following form is called a quadratic programming problem:*

$$\begin{aligned} \underset{x}{\textit{minimize}} \quad & \frac{1}{2} x^T P x + q^T x \\ \textit{subject to} \quad & ax = b, \\ & Ax \leq B, \\ \textit{and} \quad & x \geq 0. \end{aligned} \tag{4.3}$$

This is in the most general form with both equality and inequality constraints.

[1] [41]
[2] [41]
[3] [31]

4.2 Nonlinear Model Predictive Controller

As mentioned before, the control methodology should reflect the nonlinear dynamics of the thermal system; moreover, as the temperature and actuator input constraints play a critical role in the BTMS control problem, NMPC, with its significant constraint handling capability [66], [84], is selected as a proper control approach.

Here, the NMPC controller is formulated as an optimal control problem (OCP); however, it should be turned into a nonlinear programming (NLP) problem which is online implementable [100], and therefore suited to the automotive industry qualifications. The proper cost function [43] is later explained for each of the platforms.

Before presenting the controller, the properties of the system's mathematical model should be pointed out. In this regard, we should first consider the following assumptions, merely for the purpose of this study:

Assumption 1 *$\mathcal{X} \subseteq \mathbb{R}^n$ and $\mathcal{U} \subseteq \mathbb{R}^m$ are the state and control spaces, respectively.*

Assumption 2 *$\mathcal{X}$ and $\mathcal{U}$ are considered as independent matrix spaces. They also show the feasible region for state and input, respectively.*

As it was observed previously, the battery system dynamics can be well described by an ordinary differential equation (ODE), which in a discrete form becomes

$$x(k+1) = f(x(k), u(k)). \tag{4.4}$$

The map $f : \mathcal{X} \times \mathcal{U} \mapsto \mathcal{X}$ is the state transition function, where $x(.) \in \mathcal{X}$ and $u(.) \in \mathcal{U}$ denote the state and control sequence, and k represents the time step.

To have this system track the desired reference state, a finite horizon OCP defined as

$$\begin{aligned} \underset{u(.)\in\mathcal{U}}{\text{minimize}} \quad & J_N(k, x_k, u(.)) = \sum_{j=k}^{k+N-1} \ell(x^u(j, x_k), u(j)), \\ \text{subject to} \quad & x^u(j+1, x_k) = f(x^u(j, x_k), u(j)), \\ \text{and} \quad & x^u(j, x_k) \in \mathcal{X}, \end{aligned} \tag{4.5}$$

is solved at each time step k. Here, subscript N shows the prediction horizon, x_k and $x^u(., x_k)$ represent the state and the predicted state-trajectory at time k, and $\ell : \mathcal{X} \times \mathcal{U} \mapsto \mathbb{R}^+$ is the instantaneous cost functional. Before moving on, another assumption should be added as the contract:

Assumption 3 *For simplicity and throughout this thesis, by stating $x(.) \in \mathcal{X}$ and $u(.) \in \mathcal{U}$, we actually mean that $x(.)$, $u(.)$ remain inside the feasible region, so that we would not have to check feasibility as one of the constraints. In fact feasible region is merely defined by the inequality constraints in this problem.*

4.2.1 Discretization Scenarios

There are different techniques to deal with the above-mentioned OCP [25]. Here, the problem is reformulated under the so-called discretization procedure so that the NLP solvers could be applied for numerical solution [25], [41] with less computational effort [100]. To come up with the best design for the BTMS control, two different discretization methods, single shooting and full discretization, are explained and applied. In both of these scenarios, once the optimization problem is solved, the first element of the optimal control sequence is applied to the system. As it will be shown, the equality and inequality constraints are defined in each case, and the input/state bounds are automatically checked, as previously stated in Assumption 3.

Single Shooting

The first discretization scenario, namely the single shooting method, considers the control law sequence as the optimizer. Using this concept, Equation 4.5 can be written as

$$\begin{aligned} \underset{u(.)\in\mathcal{U}}{\text{minimize}} \quad & V_N(k, x_k, u(.)) = \sum_{j=k}^{k+N-1} \ell(x^u(j, x_k), u(j)), \\ \text{subject to} \quad & G(u(.)) = G(x^u(j+1, x_k) - \\ & f(x^u(j, x_k), u(j))) \leq 0. \end{aligned} \tag{4.6}$$

As it is observed, there is no equality constraint,

and there are $N * n$ inequality constraints, as a result of writing the state bounds in terms of the input. Moreover, $u \in \mathcal{U}$ guarantees the input feasibility (by Assumption 3).

Full Discretization

The title "full discretization" is borrowed from [41] to avoid any confusion. In this scenario, all of the states as well as the inputs are considered as minimizers. In other words, Equation

4.5 is restated as

$$\begin{aligned} \underset{(u(.)\in\mathcal{U},x^u(.,x_k))\in\mathcal{X}}{\text{minimize}} \quad & V_N(w(.)) = \sum_{j=k}^{k+N-1} \ell(x^u(j,x_k),u(j)), \\ \text{subject to} \quad & H(u(.),x^u(.,x_k)) = x^u(j+1,x_k) - \\ & f(x^u(j,x_k),u(j)) = 0. \end{aligned} \tag{4.7}$$

Here, it should be remarked that the inequality constraints, including the lower and upper bounds on the input and state trajectory, are considered as $u(.)$ and $x(.)$ and remain in the feasible region. Moreover, the system dynamics is considered as N equality constraints (Hs).

4.2.2 NLP Solver

As previously stated, the whole point of turning the OCP to an NLP was to be able to apply one of the NLP solvers to it. For simplicity, NLP is written in a concise form as [41]

$$\begin{aligned} \underset{z\in\mathbb{R}^n}{\text{minimize}} \quad & V(z), \\ \text{subject to} \quad & H_i(z) = 0 \text{ for } i \in \Gamma \\ \text{and} \quad & G_i(z) \geq 0 \text{ for } i \in \kappa, \end{aligned} \tag{4.8}$$

where Γ and κ show the set of indices of the equality and inequality constraints, respectively. Equation 4.8 seeks the optimal value of z, namely z^*, such that the cost becomes minimum. This problem can in fact be translated into constructing a sequence of z's moving towards z^*. To find such a sequence, the NLP is turned into a quadratic programming (QP) problem (Definition 1); the cost function is quadratically approximated in the vicinity of the existing point as Theorem 2 suggests, with the constraints being approximated linearly through Theorem 1.

Choice of solver depends on the problem and goals in each specific application. Two popular solvers in this regard are the active-set sequential quadratic programming (SQP) methods and interior-point (IP) algorithms. Detailed steps of the solution are fairly inspired from that offered by [41]. We start with explaining the easier form, namely the unconstrained problem. We then provide the necessary background and solution of the constrained case, which is in turn categorized as equality and inequality constrained optimization. Even though both solvers facilitate turning the inequality constrained problem into an equality constrained one, first the main steps of the IP strategy are described;

the implementation procedure, in terms of the applied methods and the approximations, is similar to that in fmincon of MATLAB [8]. Many of the steps are the same in SQP; thus, we mention the details of IP first, and then explain its differences with those of SQP briefly.

Unconstrained Problem

To get started, we first consider an unconstrained optimization problem as

$$\underset{z\in\mathbb{R}^n}{\text{minimize}} \quad V(z). \tag{4.9}$$

Starting from an initial guess, or z_0, here the goal is to construct a sequence that converges to z^*. This sequence can be found using two different approaches, namely line-search and trust region methods [41].

In the vicinity of each iterate z_k within the sequence, the above-mentioned unconstrained problem can be modelled using Theorem (2), or in other words

$$V(z_{k+1}) = V(z_k) + d_k^\intercal \nabla V(z_k) + \frac{1}{2} d_k^\intercal B_k d_k, \tag{4.10}$$

where B_k is the Hessian ($\nabla^2 V(z_k)$) or its approximation, and d_k is the search direction. When minimized with respect to d_k, this quadratic function gives the optimal direction. By means of this direction, the line-search methods determine the next iterate z_{k+1} as follows:

$$z_{k+1} = z_k + \alpha_k d_k, \tag{4.11}$$

where α is the step length. It could be calculated by the following one-dimensional minimization:

$$\underset{\alpha_k>0}{\text{minimize}} \quad V(z_k + \alpha_k d_k). \tag{4.12}$$

Trust-region methods, merely apply the direction to construct the sequence;

$$z_{k+1} = z_k + d_k. \tag{4.13}$$

Both of the techniques are available in MATLAB fmincon as well.

Constrained Problem

In case of the constrained problem, or Equation 4.8, the cost function is modified by integrating the constraints into it. Definition of so-called Lagrangian function as follows facilitates such a modification:

$$L(z, \lambda_1, \lambda_2) := F(z) - \lambda_1^\intercal H(z) - \lambda_2^\intercal G(z), \tag{4.14}$$

where vectors $\lambda_1 \in \mathbb{R}^{n_h}$ and $\lambda_2 \in \mathbb{R}^{n_g}$ are called the Lagrangian multipliers, compensating violation of each of the constraints in a sense. After defining the Lagrangian function as above, Karush-Kuhn-Tucker (KKT) can be applied to check the necessary condition of optimality for a constrained optimization problem [38].

Theorem 3 ***Optimality Necessary Condition***
Consider Equation 4.8 and z^* as its local minimizer, where functions V, G, and H are continuously differentiable and constraint-function gradients (∇H and ∇G) are linearly independent. Then there exist Lagrangian multipliers ${\lambda_1}^*$ and ${\lambda_2}^*$ such that the following conditions hold:

$$\nabla L(z^*, {\lambda_1}^*, {\lambda_2}^*) = 0, \tag{4.15}$$

$$H_i(z^*) = 0 \text{ for } i \in \Gamma, \tag{4.16}$$

$$G_i(z^*) \geq 0 \text{ for } i \in \kappa, \tag{4.17}$$

$$\lambda^*_{2,i} \geq 0 \text{ for } i \in \kappa, \tag{4.18}$$

$$\lambda^*_{1,i} H_i(z^*) = 0 \text{ for } i \in \Gamma, \tag{4.19}$$

$$\lambda^*_{2,i} G_i(z^*) = 0 \text{ for } i \in \kappa. \tag{4.20}$$

Now the sufficient optimality condition can be stated through the following Theorem:

Theorem 4 ***Optimality Sufficient Condition*** *[38] Given a feasible point z^* and Lagrangian multipliers ${\lambda_1}^*$ and ${\lambda_2}^*$ fulfilling KKT conditions, if*

$$v^\intercal \nabla^2 L(z^*, {\lambda_1}^*, {\lambda_2}^*) > 0 \tag{4.21}$$

for all $v \neq 0$, then z^* is strictly a local minimizer of Problem 4.8.

Inequality and Equality Constrained QP

As observed in Equation 4.8, NLP is formulated in a very general case, where V, H, and G could be any nonlinear function. As for solving the optimization problems, however, these functions are approximated properly to result in a QP problem, to which IP or SQP is applied. The basic idea in both IP and SQP is to turn the inequality constrained problem into an equality constrained one; IP does so using the so-called slack variables. On the other hand, active-set methods are based on considering a set with the subscripts of the active constraints at each time step and updating it throughout the solution. In both of the cases, the KKT conditions are applied to this reformulated QP, and the resulting system of equations is solved to give the sequence converging to the optimal solution. We first explain the procedure for the IP method; because many of the steps are similar in both of the methods, SQP algorithm is briefly mentioned afterwards.

IP Procedure

As for the IP case, the NLP problem is redefined as

$$\begin{aligned} \underset{z\in\mathbb{R}^n,\ s\in\mathbb{R}^{n_g}}{\text{minimize}} \quad & V(z) - \mu \sum_{i=1}^{n_g} \ln(s_i), \\ \text{subject to} \quad & H_i(z) = 0 \text{ for } i \in \Gamma, \\ \text{and} \quad & G_i(z) - s_i = 0 \text{ for } i \in \kappa \textit{ and } s_i \geq 0, \end{aligned} \tag{4.22}$$

which is called the barrier approach [41]; here $s_i \geq 0$ represents the slack-variable associated with the i^{th} inequality constraint. Minimizing the barrier term guarantees staying away from the boundaries, as the smaller s becomes, the closer to the boundaries the solution is. Throughout the procedure, in addition to the sequences of z and s, Lagrangian multipliers are calculated. Moreover, a sequence is found for $\mu > 0$ which converges to zero. To solve this problem, two different categories of techniques, namely conjugate gradient and direct-step methods (CGMs and DSMs), can be applied. The idea is pretty similar to that discussed earlier regarding trust-region versus line-search methods; as opposed to the CGMs where only a $1D$ optimization problem is being solved, in DSMs one should calculate both the search direction and step length, as the case in line-search.

In CGMs, the equivalent QP problem can be written as follows [4]:

$$\begin{aligned} \underset{d_z\in\mathbb{R}^n,\, d_s\in\mathbb{R}^{ng}}{\text{minimize}} \quad & d_z^\intercal \nabla V(z_k) + \frac{1}{2} d_z^\intercal B(z_k) d_z + \mu e^\intercal {S_k}^{-1} d_s + \frac{1}{2} d_s^\intercal {S_k}^{-1} \Lambda_k d_s, \\ \text{subject to} \quad & H_i(z_k) + \nabla H(z_k) d_z = 0 \text{ for } i \in \Gamma, \\ \text{and} \quad & G_i(z_k) - s_i + \nabla G(z_k) d_z - d_s = 0 \text{ for } i \in \kappa \; and \; s_i \geq 0, \end{aligned} \tag{4.23}$$

where $S = diag(s)$, $\Lambda = diag(\lambda_2)$, and $e = ones(n_g, 1)$. To take care of the constraints, norm of the constraints is minimized inside a trust-region and a residual is found. Further details regarding this procedure is beyond the scope of this research [5].

As for DSMs, the KKT conditions are applied to the Lagrangian function of the barrier problem 4.22, resulting in a system of equations as follows [6]:

$$\begin{pmatrix} \nabla^2 L_\mu & 0 & -\nabla H^\intercal & -\nabla G^\intercal \\ 0 & S\Lambda & 0 & S \\ -\nabla H & 0 & Id & 0 \\ -\nabla G & S & 0 & Id \end{pmatrix} \begin{pmatrix} d_z \\ d_s \\ d_{\lambda_1} \\ d_{\lambda_2} \end{pmatrix} = - \begin{pmatrix} -\nabla V - \nabla H^\intercal \lambda_1 - \nabla G^\intercal \lambda_2 \\ \lambda_2 - \mu e \\ -H \\ -G + s \end{pmatrix}, \tag{4.24}$$

where $\nabla^2 L_\mu$ is the Hessain of Lagrangian of the barrier problem, Equation 4.22. There are different approaches to solve this system of equations; MATALB fmincon uses an LDL factorization, where positive definiteness of the Hessian is also checked, and the algorithm switches to CGM if the Hessian is not positive definite (PD) [8].

Here, Null-space approach, as a method without matrix-inverse calculation, has been chosen over LDL factorization. There exist a great deal of literature on null-space methods [69], and here the algorithm for quadratic problem with linear constraints has been applied [48]. Moreover, to medicate the issue of non PD Hessians, quasi-Newton methods can be applied[7].The term Quasi-Newton Method goes back to the methods that consider an approximation of Hessian instead of the Hessian. Here Broyden-Fletcher-Goldfarb-Shanno (BFGS) algorithm is used for updating the Hessian [38]. Based on this method, Hessian is updated as follows:

[4] Step-by-step proof is provided in [41]. The final problem is formulated similar to MATLAB's approach [8]

[5] The detailed procedure can be found in [41]

[6] There are several ways to write and interpret this system of equations; however, here the formulation used by MATLAB [8] has been applied as it facilitates a simpler implementation.

[7] There are other ways to fix this issue as well. For example, [41] suggests adding an extra term δId to Hessian.

$$B_k = B_{k-1} + \frac{vv^\intercal}{v^\intercal \Delta x} - \frac{B_{k-1}\Delta x \Delta x^\intercal B_{k-1}}{\Delta x^\intercal B_{k-1} \Delta x}; \tag{4.25}$$

where $\Delta x = x_k - x_{k-1}$ and $v = \nabla V_k - \nabla V_{k-1}$.

4.2.3 NMPC for PHEV

The main goal is to design a thermal management system which benefits from the advantages of MPC. For each of the platforms, the objective function of the MPC controller is chosen to address particular concerns. Another critical aspect of the controller design is properly defining physical constraints, as they play a critical role in this problem. As for PHEV, the idea behind optimization is to regulate the temperature and keep the coolant velocity as low as possible at the same time. Also, the state and input constraints are considered based on the physical limitations of the system, as well as the functional requirements. The last control parameter that should be designed is the temperature at which the predictive controller starts working, or T_{act}.

Optimization Objectives

As previously mentioned, the control input to the system in this case is the air velocity, by calculating which the NMPC-based controller achieves temperature tracking. Tracking can be considered by minimizing an error term, namely the difference between actual and desired temperature (T_{ref}). There should also be some considerations regarding keeping the air velocity low. Thus, to fulfil both of these objectives, at each time step k an instantaneous double-objective cost function can be expressed as

$$\ell(k, x, u) = \lambda(T(k) - T_{ref})^2 + \gamma v^2(k), \tag{4.26}$$

where the first term in the right hand side (RHS) takes care of the error between the actual and reference temperature, and the second RHS term is in charge of the control effort minimization. The weighting factors γ and λ facilitate a trade off between the two objectives.

A modified cost function can be formulated as follows:

$$\ell_1(k, x, u) = \lambda_1 T(k)^2 + \gamma_1 v^2(k) \tag{4.27}$$

where γ_1 is a constant, and λ_1 can be found using

$$\lambda_1 = a + bexp[(T(k) - T_{ref})], \tag{4.28}$$

with a and b being constants. Such formulation facilitates a temperature-adaptive reference tracking and is applied for the HIL experiment.

Physical Constraints

The state and input feasible regions are dictated by both physical limitations and system requirements. Here, based on the operating condition, the state feasible region is considered as $\mathcal{X} = [25, 40]$ (temperature in terms of ^oC). Moreover, the control input is bounded, as it represents the air velocity of an actual fan; therefore, the control feasible region can be stated as $\mathcal{U} = [0, V_{max}]$, where V_{max} is the maximum air velocity in terms of m/s, and it is one of the controller parameters that can be changed in different simulations.

Controller Implementation

The controller is implemented in Simulink. It is structured as a user-defined function block such that the load current prediction (up to N_P time steps ahead), the ambient temperature, which is assumed to be constant in this case, and the temperature feedback from the high-fidelity model block are the inputs. The output is a vector of dimension N_C, comprising of the optimal control laws. Here, as for the tradition in MPC, only the first value of such optimal inputs is applied to the model. Inside the controller the mechanism is as follows: an activation temperature, namely T_{act}, is considered, identifying when the predictive controller activates. When the battery temperature exceeds T_{act} , the predictive controller starts working, and the devised cost is minimized to give the optimal control laws. The initial condition considered by the solver is the calculated control-law vector at the previous step, which is fed back into the block. Inside the controller block, the cost is modelled as a MATLAB function. At each time-step, the user-defined control function calls the error and minimizes it with respect to the optimizers; the system dynamics as well as the constraints are also considered as MATLAB functions to be called whenever necessary.

It is worth mentioning that at low temperatures cooling is not necessary, and thus using the above-mentioned controller activation strategy avoids imposing excessive computational effort to the system. It will be observed in next chapter that this choice is of profound importance, as in certain driving scenarios the temperature rises fast, and it has to be assured that the battery temperature remains in safe region. $T_{act} = 25^oC$ is observed to perform well for most of the cases.

As previously observed, the control-oriented model is a piece-wise function, where due to its form, $V = 0$ should not happen over the prediction horizon. This is taken care of

as the high-fidelity model has an activation key for the control-oriented model; when not activated, the system switches to the Autonomie model, as already shown in Figure 3.9. Another issue is that the solver is implemented such that it uses the control laws found in the previous step. Thereby, it should be assured that none of such values are zero. An input lower bound ϵ is therefore considered, and once the controller is used, V cannot be zero.

4.2.4 NMPC for EV

In an EV, the battery is the only energy supplier, and its temperature deviations highly affect the vehicle range. The vehicle range ,therefore, becomes intertwined with the BTMS performance. Here the optimization problem constitutes allocating part of the battery power to heating or cooling the battery, so that it tracks the desired temperature trajectory. The main difference between this problem and that of PHEV is that here the cost function should account for the vehicle range as well.

Optimization Objectives

In this case, the thermal management is facilitated through minimizing the reference tracking error with respect to the tempering power. Moreover, the electric range is taken care of by considering final SOC as an optimization objective. An instantaneous cost function such as the following can be considered:

$$\ell(k, x, u) = \lambda(T(k) - T_{ref})^2 - \gamma S\dot{O}C(k). \tag{4.29}$$

Here, the first RHS term minimizes the tracking error, and the second one takes care of the final SOC [8]. In fact adding the effect of SOC time-variations to the objective function also results in a smoothness of SOC profile, and indirectly improves the battery life as the battery temperature follows the intended trajectory. This additional term will also impose restrictions on the battery power devoted to tempering; therefore, the battery ends up following the desired temperature with a minimum cost. Again, the weighting factors make a trade-off between the objectives possible.

[8] Integration of $S\dot{O}C$ over the whole time gives the final SOC, as $\int_{t_0}^{t_f} S\dot{O}C dt = SOC(t_f) - SOC(t_0)$ where $SOC(t_0)$ is a constant

Physical Constraints

While the problem is solved numerically, it should be ensured that the solution always remains within some feasible region. In the EV case, the state feasible region is $\mathcal{X} = [25, 40] \times [0.3, 0.9]$, which represents the temperature in terms of ^oC and state of charge, respectively. The tempering power is never negative, as such a negative power is physically meaningless. Thus, a bound is considered on the input: $\mathcal{U} = [0, 1000]$ (power in $watt$).

4.3 Controller Benchmarking

A comparative study is necessary to yield insight into the advantages of the adopted NMPC-based controller. As such, other methods that are applied, including rule-based controller and PID, are explained in this section.

4.3.1 Dynamic Programming

Dynamic Programming (DP) is a MB methodology capable of finding the global optimal solution of an optimization problem. This method is offline and cannot be applied for real-time applications. Nevertheless, it provides a bench-mark for evaluating the behaviour of other controllers, in that it gives the best possible performance to be expected from a controller. DP requires information of the whole trip, including the external inputs, beforehand. The solution procedure constitutes two major stages: a backward stage and a forward one. First, through the backward algorithm the cost over the whole trip is computed to decrease the computational effort; then, via the forward algorithm the cost corresponding to the initial conditions is found based on the results of the previous stage.

Prior to solving the problem, the feasible control inputs and states are discretized properly; the trip is then divided into N equal time-steps, in each of which all possible combinations of discrete state values are considered as nodes. The number of nodes at each step is denoted as M, and the number of control inputs is shown by P. Based on the Bellman's principle of optimality [46], one can claim that at an arbitrary time-step $N-k$ the minimum cost for a given state vector $X_{i,N-K}, i = 1, ..., M$ subject to the control input $U_{j,N-k}, j = 1, ..., P$ becomes [57]

$$J_{N-k}(X_{i,N-k}) = g(X_{i,N-k}, U_{j,N-k}) + J^*_{X_{i',N-k+1}}. \tag{4.30}$$

In fact $J_{N-k}(X_{i,N-k})$ can be translated as the cost of K final steps of an N-step process. The first term on the RHS of Equation (4.30) is the instantaneous cost at step $N-k$,

which is a function of the input and state at that time-step. The second term, $J^*_{X_{i',N-k+1}}$, represents the minimum cost associated with the upcoming state vector at the next time-step, $X_{i',N-K+1}$. This minimum cost for the given set of states $X_{i,N-k}$ at time step $N-k$ can be obtained by

$$J^*_{N-k}(X_{N-k}) = g(X_{N-k}, u^*_{N-k}) + J^*_{N-k}(X_{N-k+1}), \tag{4.31}$$

where u^*_{N-k} is the control law that minimizes J_{N-k}. It is obtained by trying all of the admissible input values and comparing their resulting costs.

As for the first stage of DP, starting at the last time-step, or N, the cost at each of the nodes, namely J^*_N, is calculated and saved [9]. Then we go one step back, step $N-1$, and calculate J^*_{N-1} for all of the nodes, using Equation 4.31. The same procedure is then repeated for every time-step all the way back to the very beginning of the trip, where the minimum cost and optimal input values are saved for every node.

As for the forward-stage, one would start from the state initial condition and apply the optimal input associated with them to calculate the states of the next time-step. The optimal control laws for these calculated states are applied. This procedure is continued until the last time step, and eventually the appropriate control strategy for the problem is found.

4.3.2 PID Controller

PID controllers have been successfully applied in industry for a variety of tracking tasks [94]. Thus, it is chosen as one of the bench-mark methods here; Simulink PID block is used, which linearly approximates the plant and then automatically tunes the controller. For manually tuning the controller, one would normally start with the proportional gain, then uses the derivative term to improve the time behaviour of the response and eventually the integral term to address the steady-state error.

4.3.3 Rule-based Controller

Rule-based controllers are reliable yet simple controllers, frequently used in industry, where their rules are basically obtained through years of experiment. As for BTMS in PHEVs, different rule-based algorithms have been applied, mostly activating fan below 35^oC. This

[9] Unless the cost function has a terminal cost or a term which is merely a function of states, this value is zero, which is also the case in this study.

idea is also applied here to examine how much improvement NMPC provides compared to the conventional rule-based. As for EV, this way of formulating the BTMS is new, and a realistic rule for benchmarking is not at hand.

Chapter 5

Controller Evaluation

In this chapter, simulation results are provided to demonstrate the potential of MPC for thermal systems with their slow nature; specifically, the problem is formulated as NMPC, due to the nonlinearities of thermal systems. The designed controllers are then evaluated through MIL simulations and HIL experiments. Moreover, other benchmark methods have been used to provide a more concrete examination of the NMPC-based controller benefits.

This chapter is organized as follows: first the maximum potential of the existing systems is identified. In case of PHEV, two sets of simulations, one with fan on all the time and the other with a DP-based controller, are conducted to accommodate this goal. As for EV, DP-based controller is used in this regard. Next, the NMPC controllers are applied to both of the platforms, and the results are compared with those of the benchmark methods. In PHEV, this is also backed-up with MIL and HIL test-benches, and general rules are sought regarding proper settings of NMPC for different trip scenarios. Nonetheless, for EV the controller performance over the control-oriented model is examined.

5.1 Maximum Potential of the System

The goal in this section is to investigate the maximum capability of the existing BTMSs in each of the baseline platforms. Having such information prior to testing the predictive controllers provides insight into the realistic results that could be expected from them.

5.1.1 PHEV

As for the baseline PHEV, there are two aspects to be investigated: the optimal control-laws, or the global optimal solution of BTMS problem, and the actuator potential, which can be recognized by applying the actuator's maximum power. These aspects are particularly important, as in any driving scenario it should be assured if the BTMS could be modified by merely changing the control strategy, or the actuator has to be replaced.

In the following, the actuator potential as well as optimal control strategy are investigated by providing simulation results with fan on all the time and DP-based controller, respectively.

Results with Fan On All the Time

As previously mentioned, the fan in the baseline PHEV is activated based on an RB strategy. This strategy works well in many cases, such as conventional city-driving-cycles; however, there exist cases that challenge the standard BTMS. Aggressive cycles[1] as well as highly variable road grades are examples of such challenging scenarios. System's behaviour over an aggressive scenario, namely four subsequent US06 driving cycles, is shown in Figure 5.1. Temperatures below $40\,^oC$ are considered acceptable. Thereby, the RB BTMS does not have a satisfactory performance in this case. Different fan velocities are examined where the fan is kept on during the simulation to see how much further the BTMS could be improved. It is observed that $V_{max} = 100\,m/s$ or $120\,m/s$ results in a reasonable temperature profile, and the fan must be upsized.

The next considered driving scenario is a highly variable road grade, namely Calgary-Vancouver route driven at a constant speed of $90km/h$. As it is illustrated in Figure 5.2, RB methodology cannot handle this situation well. However, keeping the fan on all the time has alleviated the problem as in Figure 5.3.

Dynamic Programming Results

Through simulations with fan on all the time, it was concluded that the problem with US06 scenario cannot be fixed unless the actuator is upsized. The Calgary-Vancouver case, however, could be handled very well. As such, it is worth investigating the optimal control inputs that can solve the latter case given the same upper bound on the actuator

[1]Battery thermal behaviour over aggressive cycles has been a controversial topic in BTMS-related studies, as in [102].

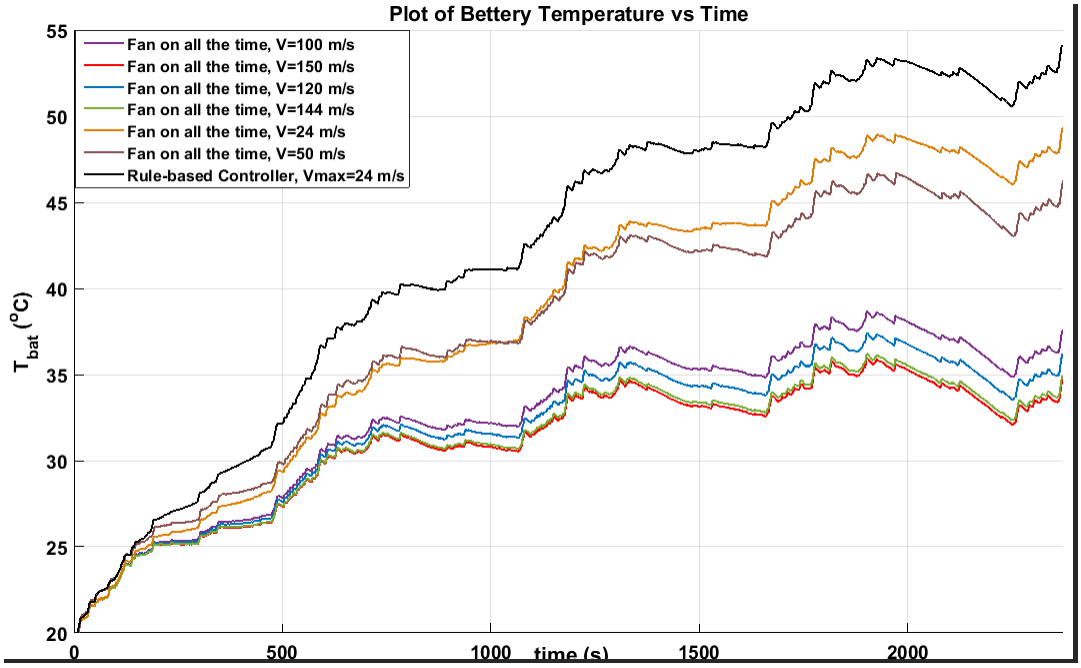

Figure 5.1: Four subsequent US06 fan on all the time. Results for different values of the velocity. Effect of changing thermal management is observed.

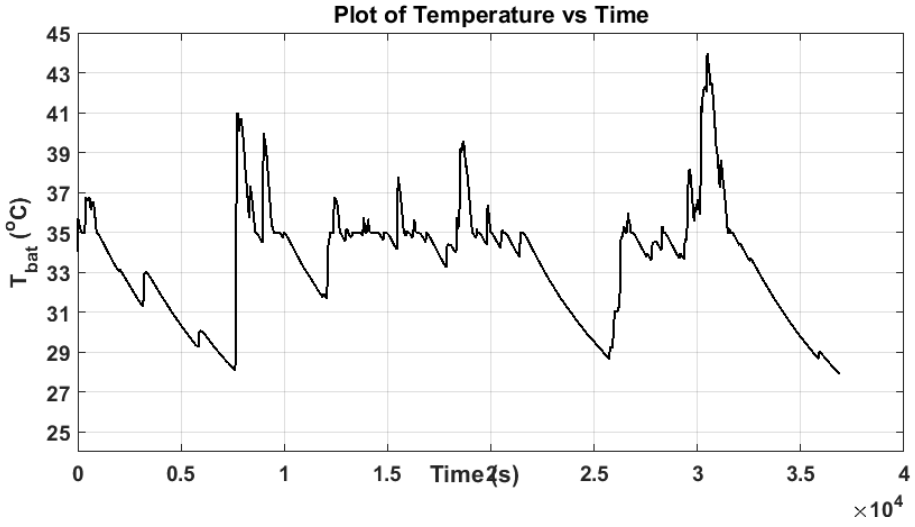

Figure 5.2: Calgary-Vancouver road. Results for the standard RB controller.

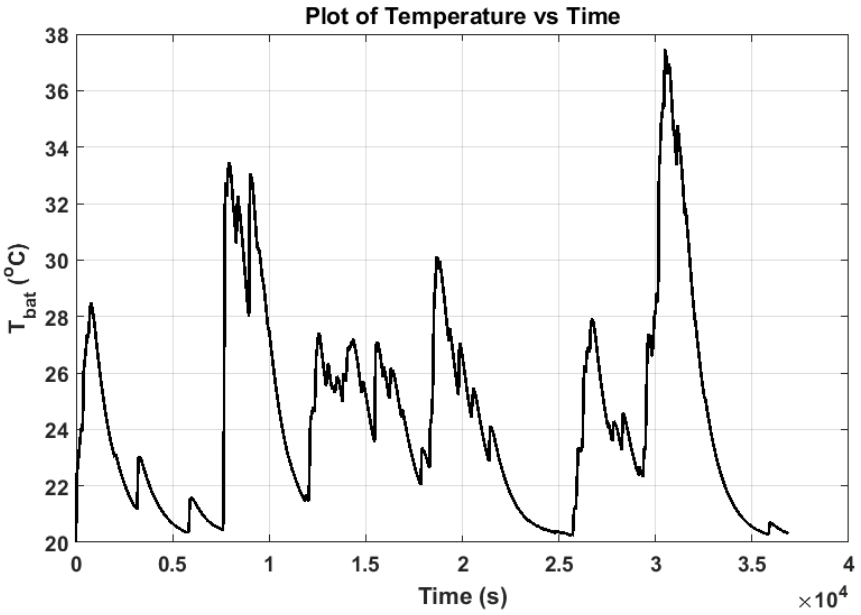

Figure 5.3: Calgary-Vancouver road. Results when fan is on all the time, with $v = 24m/s$.

input; here, DP has been applied to do so. As for the former case, such an optimization is meaningless as the existing actuator must be replaced[2].

Results of the Calgary-Vancouver case with weighting factors $w_1 = 1$ and $w_2 = 0.01$ are demonstrated in Figures 5.4 and 5.5. In the first case the upper limit of the control input is assumed to be equal to the velocity of the existing fan, whereas in the second case this value is considered 1/3 of the previous one. In both of the cases the temperature is taken care of, showing that the fan can be downsized.

5.1.2 EV

To investigate a sense of the system potential in this case, DP controller has been applied to the control-oriented model, as the BTMS-circuit model is not available. As already mentioned, the formulation in this case is based on the vehicle velocity.

[2]The velocity values were manually changed in the previous part to find the proper input value. Nevertheless, as it will be stated in the future work, for a more accurate result one could formulate the problem as simultaneous component sizing and thermal management. Existing examples of simultaneous power management and component sizing could be reformulated for thermal management as well [16].

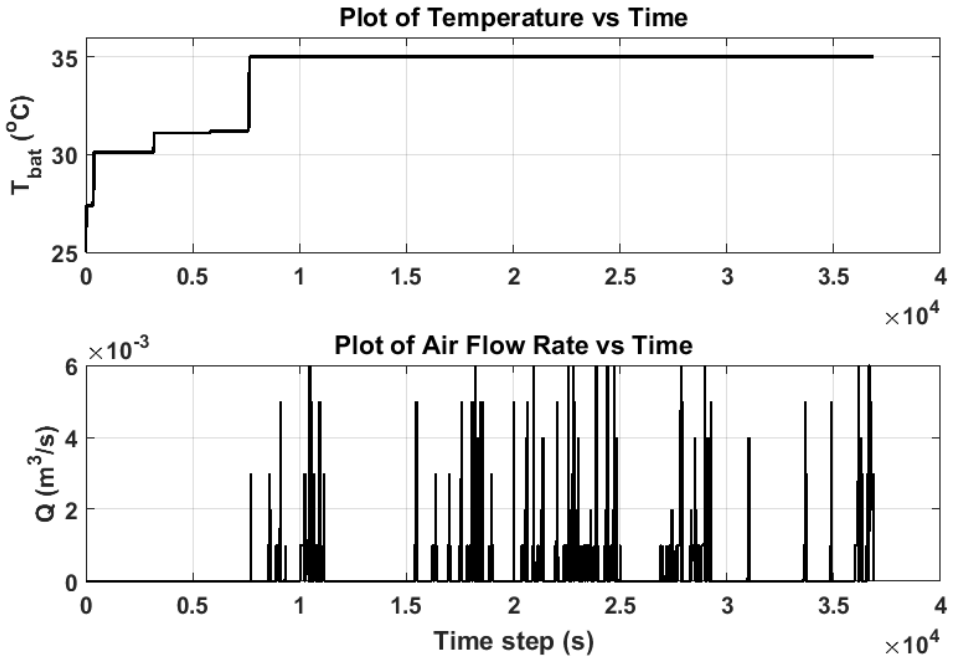

Figure 5.4: DP results for Calgary-Vancouver case, with $v = 24m/s$ or air-flow rate of $6m^3/s$.

The result for FTP-75 driving cycle is shown in Figure 5.6; it is observed that at time step 32 (1289^{th} second of the cycle), the temperature reaches the desired value of 25^oC; the tempering power, however, does not become zero at this time step, due to the objective function which accounts for the final SOC as well. The power tends to take higher values at the initial stages than it does at the final steps, and it never exceeds the assigned upper limit of $1000W$. It is also observed that SOC becomes 0.92 by the end of the process, which is 10% more than the final SOC value when there is no temperature regulation. The simulation results over US06 and an urban driving cycle are also illustrated in Figures 5.7 and 5.8, respectively, where the same trend is observed.

5.2 NMPC Performance in PHEV

In this section, the NMPC controller performance is demonstrated for the baseline PHEV.

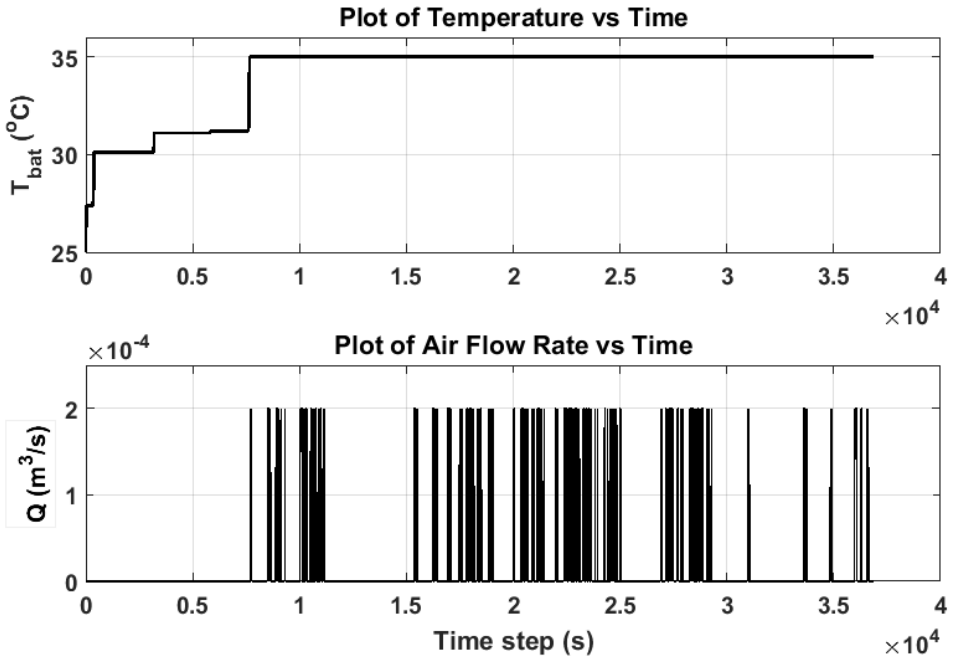

Figure 5.5: DP results for Calgary-Vancouver case, with $v = 8m/s$ or air-flow rate of $2m^3/s$.

5.2.1 MIL Simulation Results

MIL simulation diagram for the PHEV is shown in Figure 5.9. The set-up comprises of the battery high-fidelity model, controller, and a subsystem measuring the load-current, where the controller uses the temperature feedback and calculates the optimal velocity. Also, the load-current values are calculated based on the driving cycle and are assumed to be available for measurement over the prediction horizon. As mentioned in the previous Chapter, an actuation temperature, namely T_{act}, is considered inside the controller algorithm, determining when the NMPC strategy should start working. Here, to facilitate enough future information, $T_{act} = 25^oC$ is considered. This way, one could assure that the necessary prediction is available ahead of time, and the future behaviour is well observed.

In the following, simulation results of an urban cycle, namely UDDS, as well as those of the aforementioned challenging scenarios are provided.

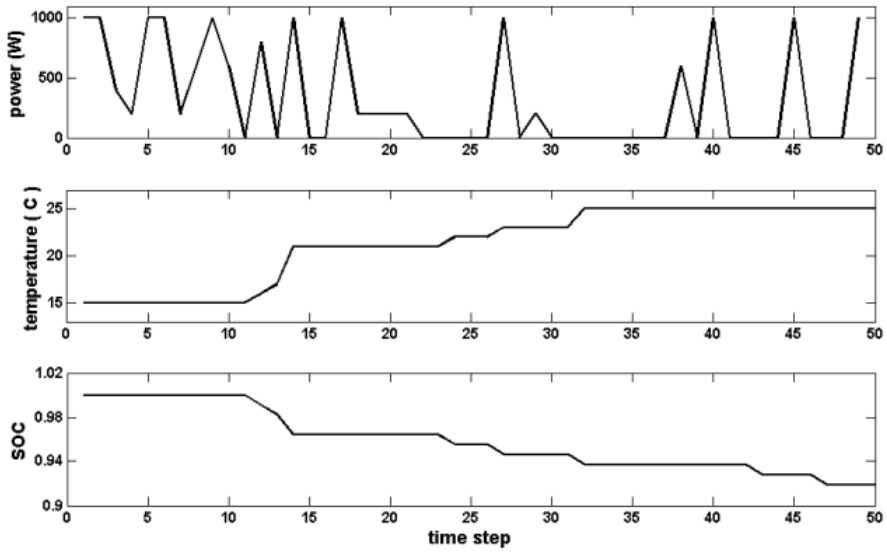

Figure 5.6: Performance of the baseline EV with the DP-based controller over FTP-75 driving cycle.

Urban Cycle

The first studied scenario is a city driving case, namely UDDS, where the controller is formulated using single shooting discretization and IP solver. The results of the devised predictive controller, with a prediction length of $10s$, as well as those of the rule-based one are shown in Figure 5.10. It is observed that in such a short period of time, replacing the default rules with the predictive algorithm significantly reduces the required control input, up to almost 80%. Moreover, despite the short duration of this cycle, the temperature profile is slightly improved.

To investigate the effect of prediction horizon, another example of NMPC application to UDDS is shown in Figure 5.11, where prediction lengths of $20s$, $200s$, and $400s$ are considered[3]. It is observed that increasing the prediction length results in earlier fan-activation, greater fan-velocity values, and less temperature rise. One could make this control strategy compatible with other driving scenarios by changing the controller's settings based on the scenario.

[3]Discussion over possibility of achieving such prediction in real-world is addressed later. Even if not possible, longer prediction horizons are worth being studied due to the knowledge of the system they offer

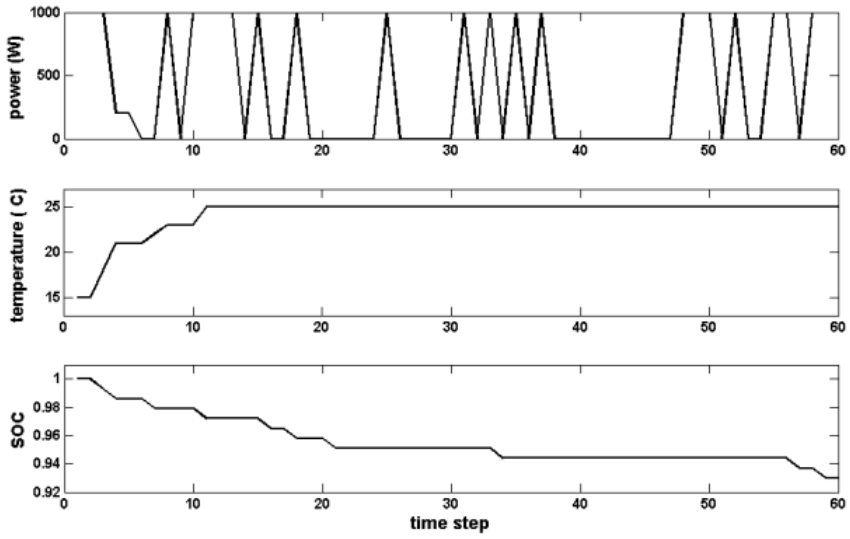

Figure 5.7: Performance of the baseline EV with the DP-based controller over US06 driving cycle.

Weighting factors used in the cost function, namely w_1 and w_2, also play a critical role here. Two general cases can be considered in this regard: single objective optimization ($w_2 = 0$) versus double-objective optimization ($w_1 = 10$ and $w_2 = 0.01$). For simulations demonstrated in Figure 5.11, $w_1 = 10$ and $w_2 = 0$. By changing both values, as in Figure 5.12, the results change; the velocity value drops to 0.1 of the former value, but temperature is not regulated as well as in the previous case. Also, non-smooth velocity behaviour observed in Figure 5.12 is a direct result of considering a non-zero weighting factor for it.

Further tuning of weighting factors is shown in Figure 5.13. It is observed that the air velocity has been decreased by changing w_2 from 0.01 to 0.001, without a significantly negative impact on the temperature tracking.

Another important factor identifying the controller performance is the turnaround time, which in this context can be defined as the time the controller takes to solve one step. It is obtained by dividing the simulation time by the total number of time-steps. Turnaround time does not necessarily decrease by increasing the prediction length, as will be observed in Table 5.1. In fact there is an optimal value for the prediction length resulting in the best turnaround time. This is because of the fact that increasing the prediction horizon

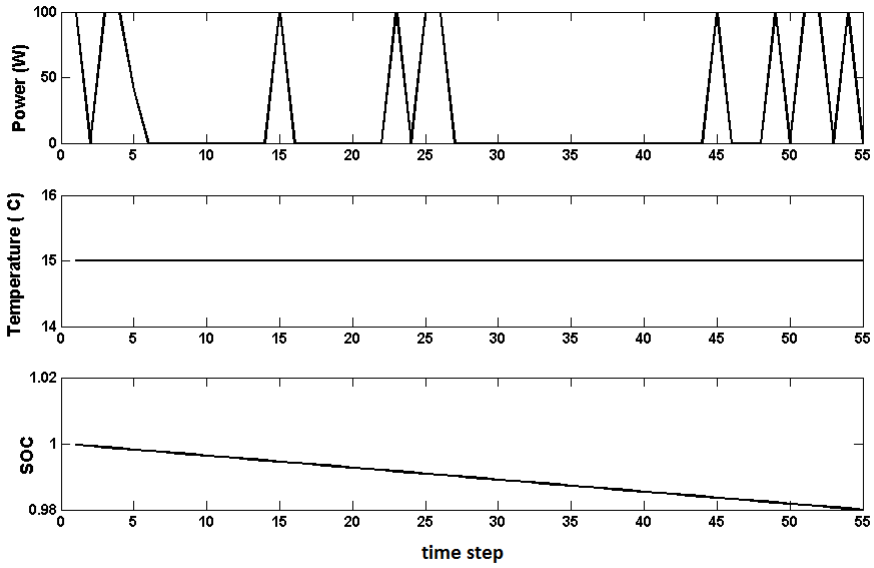

Figure 5.8: Performance of the baseline EV with the DP-based controller over a considered urban drive cycle [2].

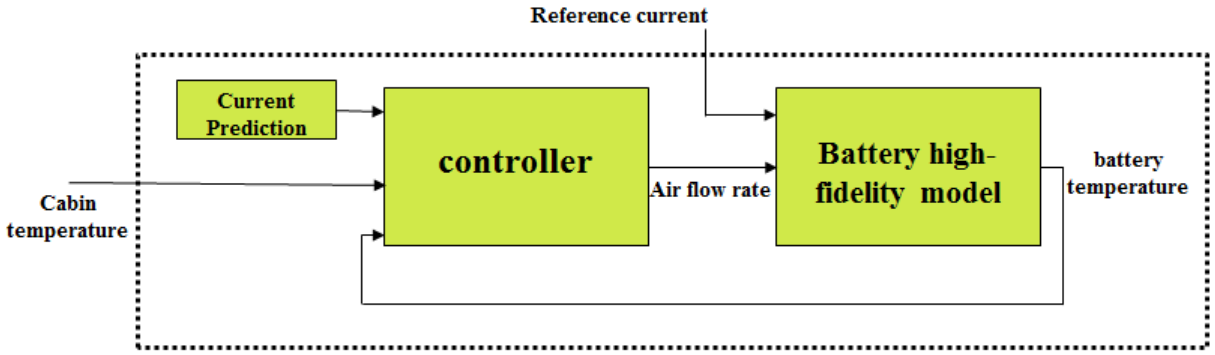

Figure 5.9: MIL Simulation Set-up in PHEV.

increases dimension of the system and could impose excessive computational cost.

It should be notified that based on the simulation results, multiple shooting method does not suggest promising results for the BTMS problem. An example of such results is demonstrated in Figure 5.14, where multiple shooting discretization scenario fails to identify the control inputs required for proper battery thermal management. This could

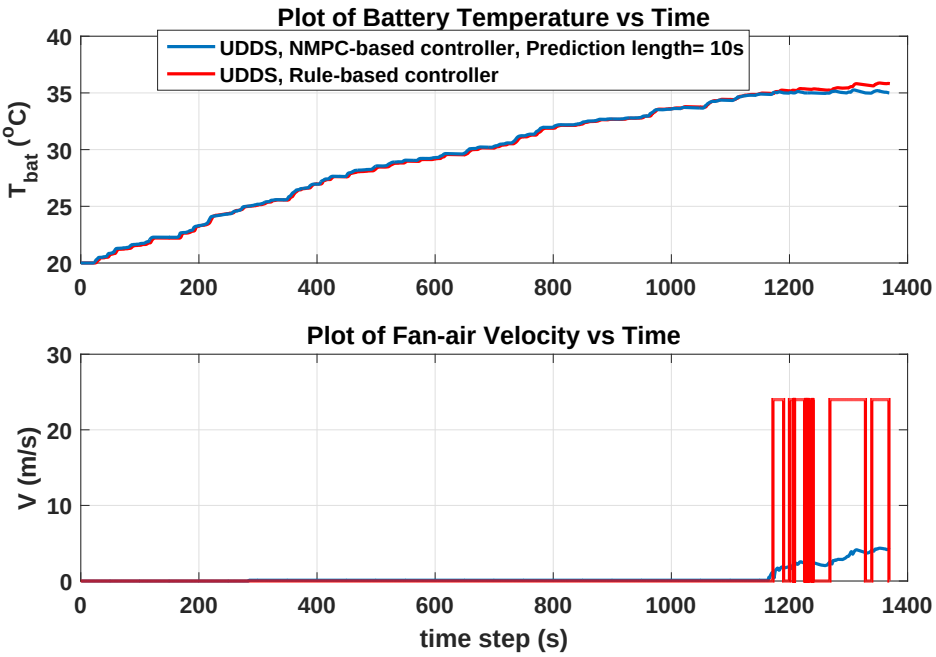

Figure 5.10: NMPC-based controller versus the rule-based one over UDDS cycle.

be related to the system scale and dimension. Thus, single shooting is considered for the rest of NMPC-based controllers applied in this research.

Challenging BTMS Scenarios

It was observed that the BTMS in the baseline PHEV failed to regulate the temperature over Calgary-Vancouver case and subsequent US06 cycles. Here, the potential of NMPC in handling those challenging scenarios is addressed; first, the NMPC controller performance over four subsequent US06 cycles is investigated. Then, the aforementioned Calgary-Vancouver case is applied to examine the controller capability.

Four subsequent US06 cycles are attached to provide a longer duration for the aggressive cycle; the results are illustrated in Figure 5.15 for different prediction horizons. To provide some room for discussion, the maximum velocity in this case is assumed to be $50m/s$ rather than $24m/s$; nevertheless, it was shown that further actuator upsizing is necessary to completely alleviate this case. Maximum realistic prediction horizon considered in this case is $50s$, which is estimated by using the $1000m$ prediction of V2V/V2I technologies,

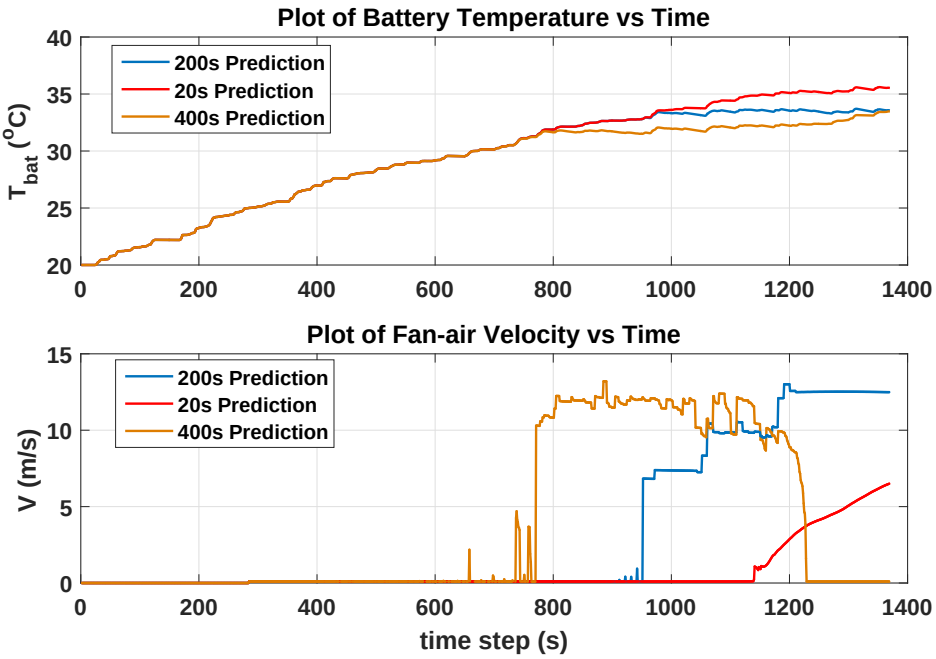

Figure 5.11: MIL simulation result: UDDS $N = 20$ single shooting interior-point solver. Results for different prediction lengths are chosen ($w_1 = 10$ and $w_2 = 0$).

provided the vehicle is driven at the velocity of 20 m/s. Changing the prediction horizon in this case has not particularly improved the controller performance. Indeed, the order of predictions must be higher to show a significant difference, and the predictive controller is insensitive to the real-life prediction ranges in case of the aggressive cycles.

To investigate the effect of the prediction horizon, longer prediction horizons, even though not realistic given the existing technology, are also considered; the simulation results are illustrated in Figures 5.16 and 5.17, where the larger the prediction length, the earlier the fan starts taking care of the situation. Nevertheless, increasing the prediction length can improve the controller regulation ability only up to a certain point. It is evident that the prediction length of $800s$ does not improve the behaviour significantly and slightly adds to the turnaround time; thus, it is a trade-off to decide what works the best. Due to the simulation results, a prediction length of around $400s$ for thermal management problem performed the best. In all of the cases in Figures 5.16 and 5.17, w_2 is equal to zero.

A comparison between the rule-based and NMPC controllers is demonstrated in Figure 5.18; the upper bound on the input has been increased to $120m/s$ to keep the temperature

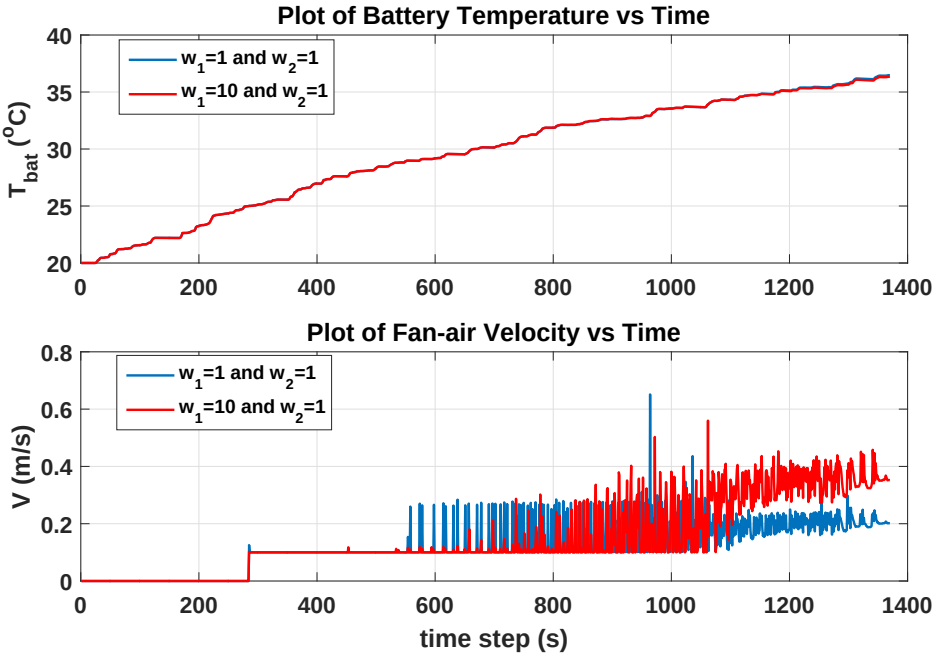

Figure 5.12: MIL simulation result: UDDS $N = 20$ single shooting interior-point solver. Results for different prediction lengths are chosen. Effect of changing weighting factors is observed.

below 40^oC. This necessitates upsizing the actuator, which should be investigated in its own sense.

The second critical scenario worth studying is the highly-variable road-grade case, or the so-called Calgary-Vancouver route. Simulation results of this case are shown in Figure 5.19 for different prediction horizons. High prediction lengths are acceptable in this case, as the road grade ahead could be approximated based on the GPS information and road maps. Based on these results, it turns out that knowing the general grade trend is necessary yet its precise value at every single point is not required. In one of the cases, the input upper bound has been increased to $100m/s$, which slightly shifts the temperature profile down. Also, the temperature profile associated with the longer prediction horizon falls below that with the lower prediction, which demonstrates the impact of predictive thermal management. This is the case without imposing significantly more value of air velocity, showing that prediction facilitates wiser application of the actuators.

Performance of the NMPC controller with $800s$ prediction length versus that of the rule-

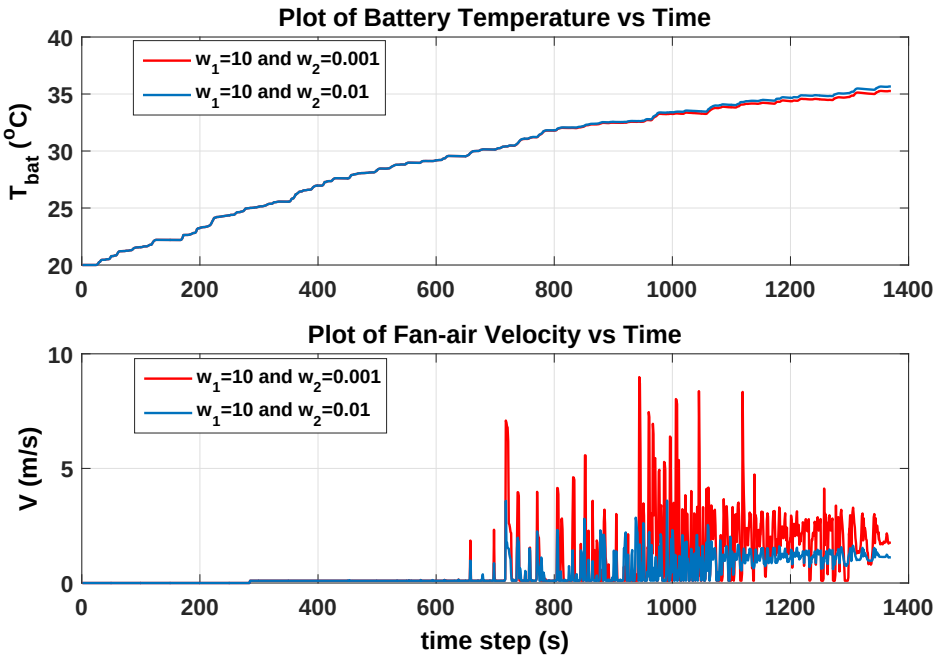

Figure 5.13: MIL simulation result: UDDS $N = 20$ single shooting interior-point solver. Results for different prediction lengths are chosen. Effect of changing weighting factors is observed.

based is shown in Figure 5.20. It is observed that the NMPC approach results in a smoother temperature profile, with less deviations from the reference temperature. Furthermore, at higher temperatures, the impact of the predictive methodology stands out.

Conclusion of the MIL Simulations

A summary of the simulation results can be seen in Table 5.1. Based on the NMPC controller simulation results, some general guidelines regarding tuning the BTMS control algorithm for the baseline PHEV can be offered, as follows:

- To take care of the aggressive cycles, one should use the maximum capability of the BTMS. As such, keeping the fan on all the time strategy is recommended. This, however could be subject to change based on the cycle duration and current gradient.
- When it comes to highly variable road grades, predictive approaches result in a better performance and are more cost-effective.

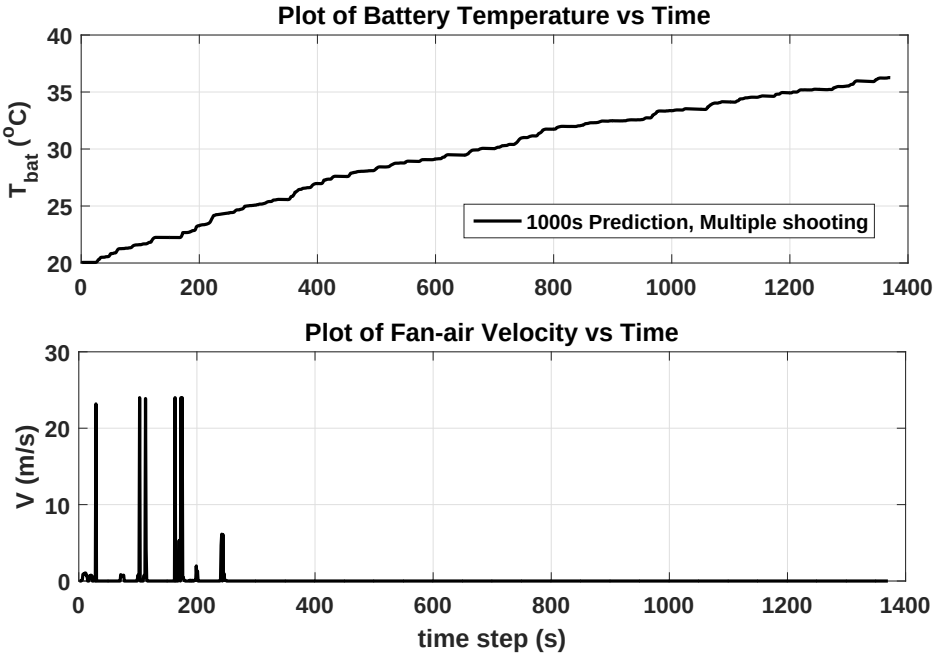

Figure 5.14: MIL simulation result: UDDS $N = 10$ multiple shooting interior-point solver.

- As for city driving, although the rule-based controller performs well, predictive approaches perform better as expected, mainly in that they save a great amount of energy.
- Choice of weighting factor is dependant on the driving circumstance. For example, the Calgary-Vancouver trip is handled well without considering a weighting factor for the input, which is not always the case.
- The NMPC should be discretized using the single shooting method.

5.2.2 HIL Results

As mentioned in the introduction, HIL experiment is applied to conduct the simulations in real-time. This is important since it identifies the applicability of the controller to real vehicles. The HIL set-up comprises of a real-time simulator and an ECU. The simulator, namely DS1006 processor board, executes the high-fidelity model, and the ECU, or in this case MicroAutoBox II, runs the controller. Signals are sent between the two of them

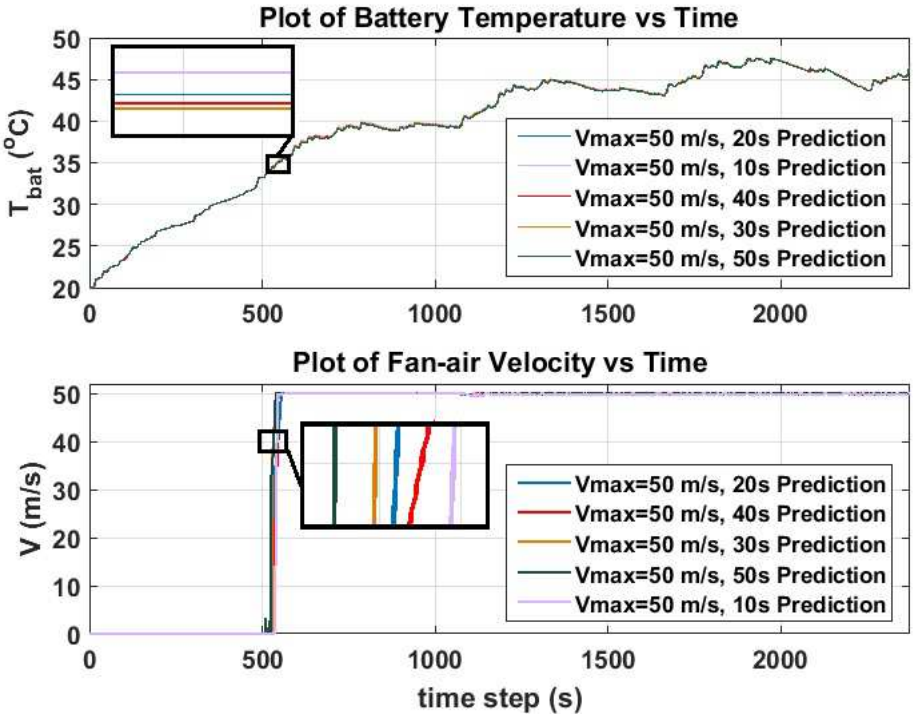

Figure 5.15: MIL simulation result: four subsequent US06 single shooting Interior-point solver. Results for realistic prediction lengths.

via Controller Area Network (CAN). The considered signals in this case are velocity and temperature feedback. Also, modified cost function (4.27) along with a GMRES-based solver [89] are used to formulate the controller. A comparison between MIL and HIL results for different cases is illustrated in Figures 5.21 to 5.23. The observed turnaround time, varying between $10\mu s$ to $1ms$, verifies the performance of the predictive controller.

5.3 NMPC Performance in EV

For EV, the results are limited to applying the controller to the control-oriented model, as a high-fidelity model is not at hand. NMPC performance over FTP75 is illustrated in Figure 5.24. Maximum tempering power is applied up to the 27^{th} time-step, where it becomes zero, as the tracking goal is fulfilled; however, one more non-zero power value is observed later. This is acceptable for there are two objectives to be taken care of. A

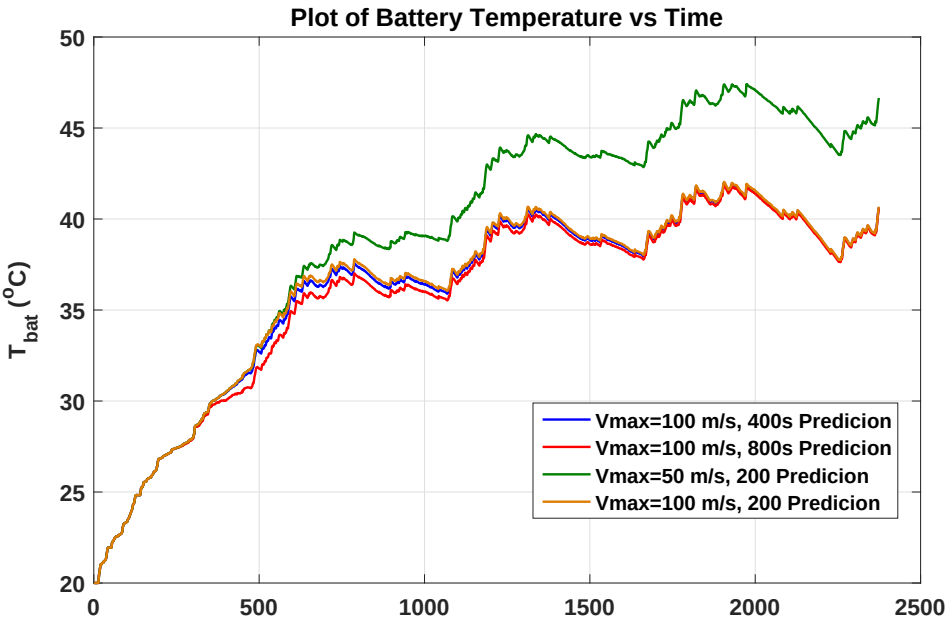

Figure 5.16: MIL Result: four subsequent US06 single shooting interior-point solver. Results for different prediction lengths and upper bound velocities.

PID controller is applied as benchmark to track the same desired temperature, as shown in Figure 5.25. Tempering power is non-zero only in the beginning of the simulation; at the 34^{th} time-step, as the temperature reaches the steady-state value, tempering power becomes zero. It can also be seen that initially the power takes an ultimately high value and reaches $3000W$ at the 2^{nd} time-step and decreases gradually thereafter. By making a comparison between the performance of NMPC-basedcontroller and that of PID in terms of reference-tracking, it turns out that although both of the controllers are capable of tracking the desired temperature well, the predictive controller results in a better performance with a less tempering-power consumption. This is because of the fact that NMPC considers constraints on the input and states, and therefore has the capacity to limit their resulting values. Also, the considered NMPC cost function ensures acquiring other objectives in addition to reference tracking. In this case, NMPC results in a smaller total value for the tempering power, enabling the battery to allocate more power to traction, and thus comes up with a higher driving range; moreover, as a result of considering SOC in its objective function, NMPC leads to a higher final SOC, which again means a higher vehicle range.

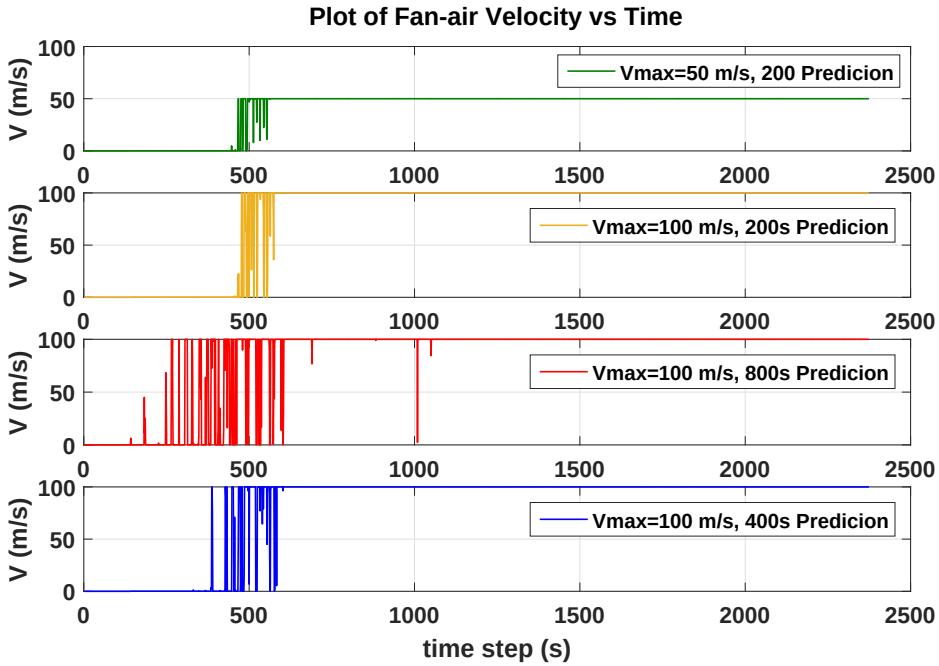

Figure 5.17: MIL Result: four subsequent US06 single shooting interior-point solver. Results for different prediction lengths and upper bound velocities.

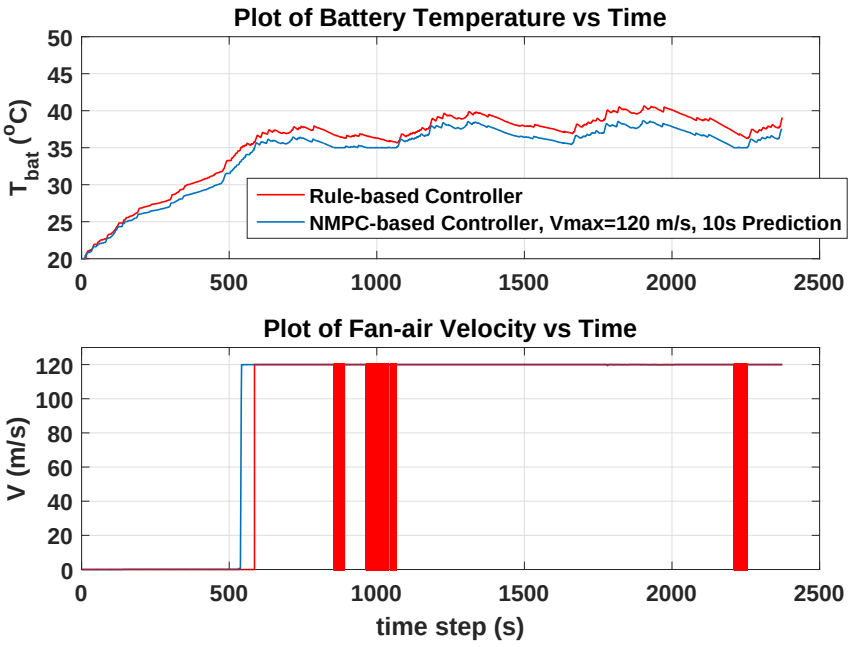

Figure 5.18: MIL Result: NMPC performance versus rule-based controller for four subsequent US06 cycle.

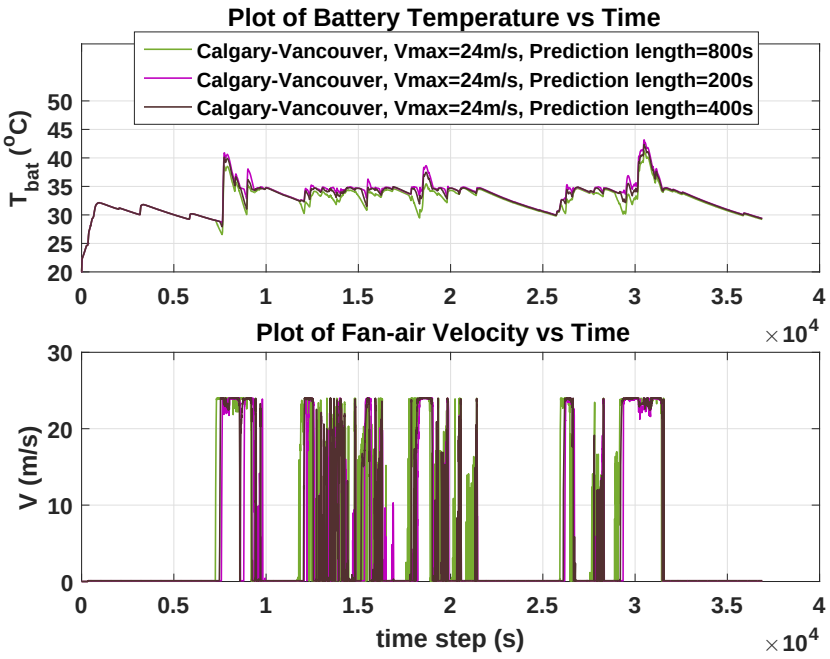

Figure 5.19: MIL Results for NMPC: Calgary-Vancouver route results with different prediction lengths.

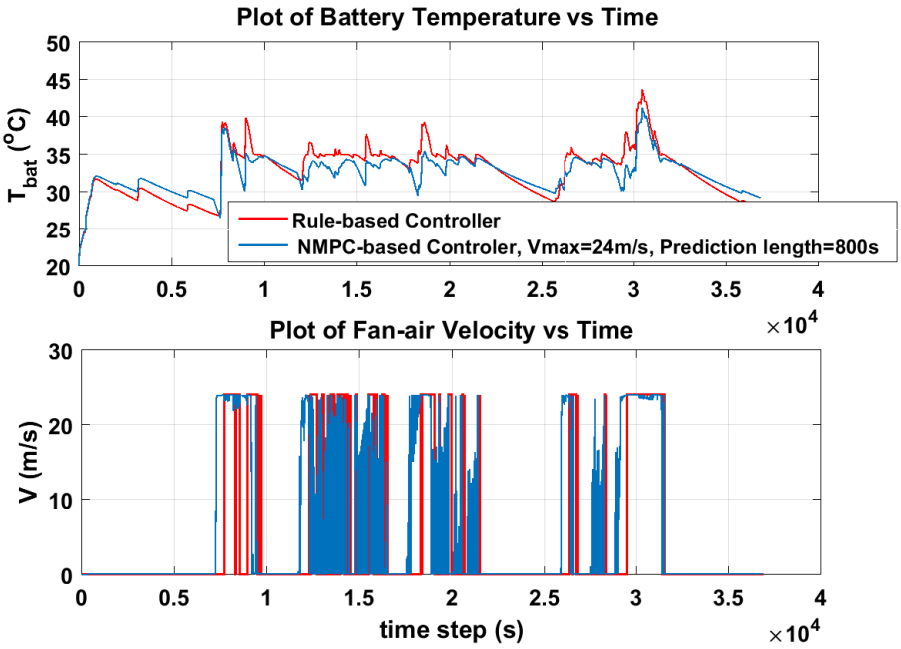

Figure 5.20: NMPC performance versus rule-based controller for Calgary-Vancouver road.

Table 5.1: MIL simulation results for NMPC-based BTMS in PHEV

Algorithm	Drive	Turnaround	Prediction	w_1	w_2	V_{max}
–	Cycle	Time(s)	Horizon(s)	–	–	(m/s)
IP	Cal-Van	0.0513	200	1000	0	24
IP	Cal-Van	0.06171	400	1000	0	24
IP	Cal-Van	0.07435	800	1000	0	24
IP	Cal-Van	0.05392	200	1000	0	24
IP	$4 \times US06$	0.08188	10	100	0.1	50
IP	$4 \times US06$	0.06928	10	1000	0	50
IP	$4 \times US06$	0.08281	10	10	0	50
IP	$4 \times US06$	0.12957	20	10	0	50
IP	$4 \times US06$	0.08054	30	10	0	50
IP	$4 \times US06$	0.07864	40	10	0	50
IP	$4 \times US06$	0.07866	50	10	0	50
IP	$4 \times US06$	0.09428	400	10	0	24
IP	$4 \times US06$	0.1407	800	10	0	50
IP	$4 \times US06$	0.1259	400	100	0	50
IP	$4 \times US06$	0.1053	400	1000	0	50
IP	$UDDS$	0.07622	20	10	0	24
IP	$UDDS$	0.06649	200	10	0	24
IP	$UDDS$	0.07318	400	10	0	24
IP	$UDDS$	0.07085	400	1	1	24
IP	$UDDS$	0.06968	400	10	1	24
IP	$UDDS$	0.07730	400	10	0.001	24
IP	$UDDS$	0.07921	400	10	0.01	24

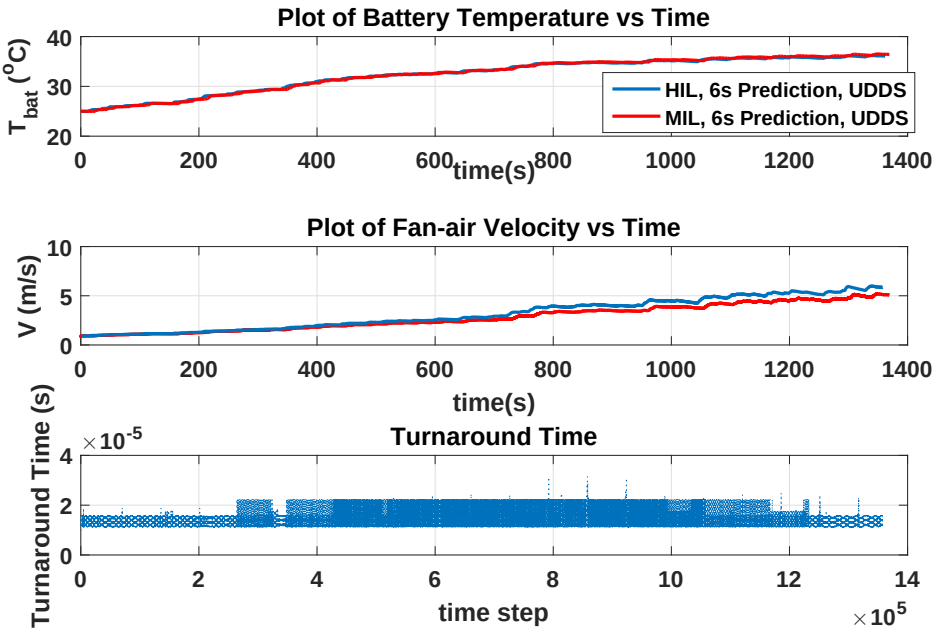

Figure 5.21: HIL results versus MIL results for UDDS cycle.

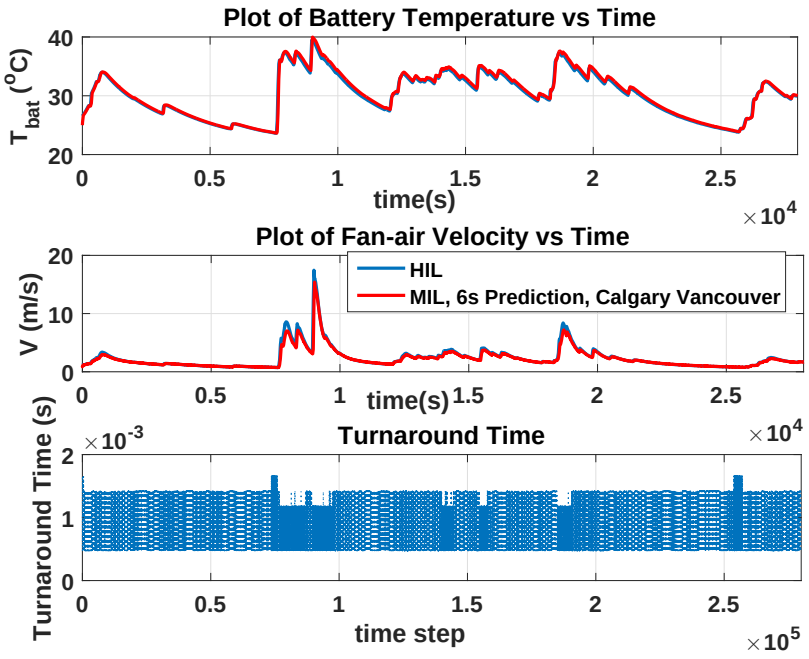

Figure 5.22: HIL results versus MIL results for Calgary-Vancouver road.

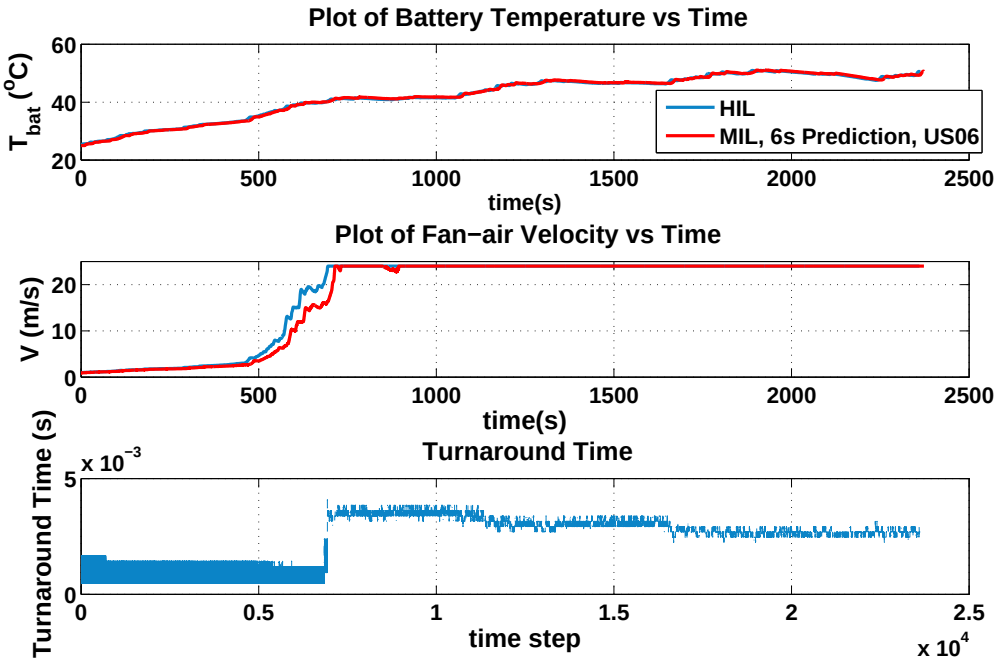

Figure 5.23: HIL results versus MIL results for US06 cycle.

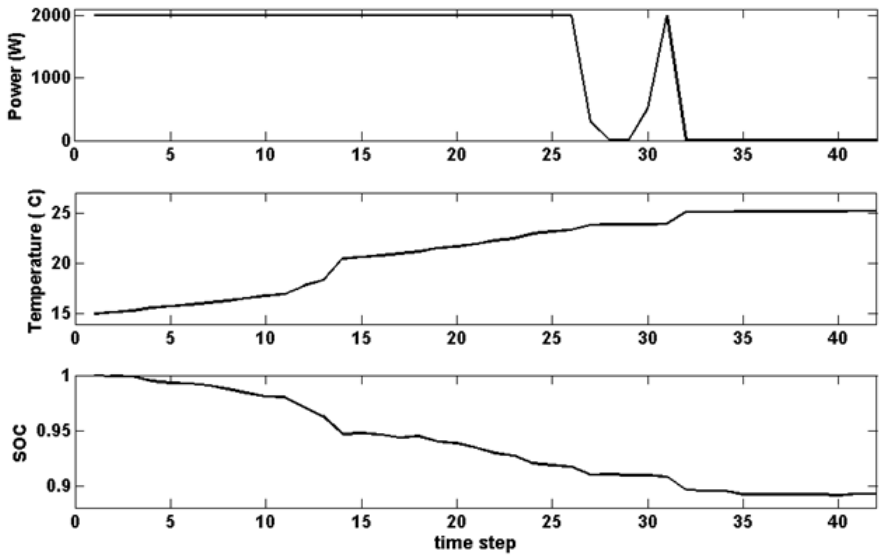

Figure 5.24: Performance of the baseline EV with the NMPC controller over the FTP-75 drive-cycle.

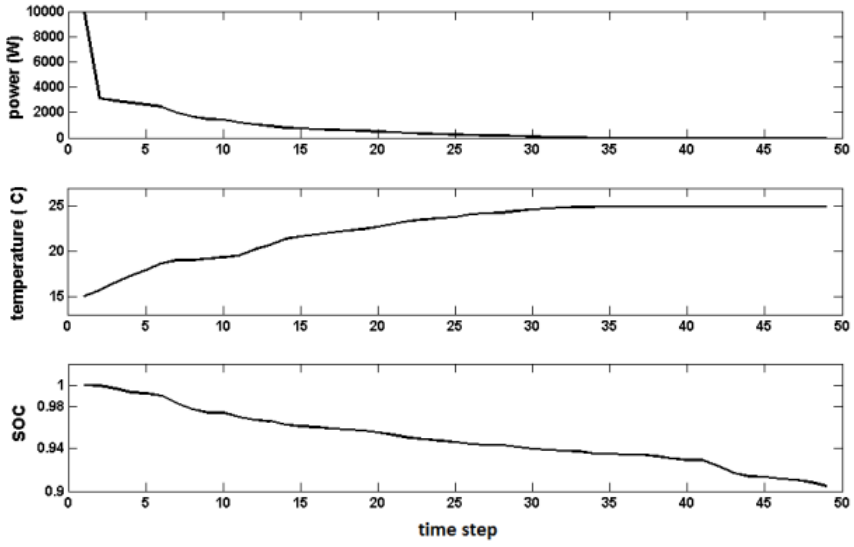

Figure 5.25: Performance of the baseline EV with the PID controller over the FTP-75 drive-cycle.

Chapter 6

Conclusion and Future Work

This chapter provides the conclusion of this thesis, followed by statement of potential areas for future work.

6.1 Conclusions

Throughout this research, a frame-work for NMPC-based BTMS control was suggested. Here, the associated major conclusions for each of the platforms are explained.

6.1.1 PHEV

The potential of NMPC in PHEV BTMS controller, as well as the requirements of a proper BTMS controller were investigated. The devised algorithm improves the BTMS control performance in the base-line PHEV, namely the Toyota Prius, as proven by simulation results over a variety of driving cycles. It is observed that the BTMS algorithm had better be switched to NMPC, specifically in case of highly variable road grades. Moreover, the turnaround time being between $10\,\mu s$ to $1\,ms$, as obtained through HIL experiment, ensures that the controller can be applied for real-time automotive applications.

6.1.2 EV

An NMPC-based controller was applied to the baseline EV, namely Toyota RAV4. The observed simulation results indicate the great potential of predictive techniques for BTMS

in EVs; in comparison with the PID controller, which is commonly applied in the industry, NMPC controller ends up tracking the reference temperature with less power and charge consumption.

6.2 Future Work

This study takes the initiative to introduce NMPC for BTMS control problem. There exist, however, various relevant areas to be considered in the future; the considered objective function could be modified such that it proposes more physical concepts; It could contain V^3 to represent a portion of the fan power. Also, the attained results ignite the research on simultaneous component sizing and thermal management, in order to identify the proper actuator size as well as the effective thermal management control strategy. The idea is very similar to the combined power train control and component sizing [49] [50]. Another promising area would be investigating the potential of MPC in simultaneous thermal management of different components including the battery pack and engine, similar to the procedure of [90]. One can even go further and add the AC system to this combination. Moreover, one could incorporate the battery end-of-life (EOL) in BTMS control, in that it should be assured that EOL does not happen before the warranty, and manufacturer's benefit is very well taken care of. This can be addressed by considering one of the many available degradation models and integrating it to the system[1]. Further, as the system is subject to many uncertainties, most importantly those caused by estimating the future power demand, studying the system robustness is a very important step before actual implementation of this mechanism on the vehicles. Different methods including robust calibration can be applied in this regard.Finally, stability of controller could be another important issue which could be studied further using persistent feasibility.

[1]One could refer to [81], which has incorporated SOC in the engine thermal management. It can be similarly done for battery thermal management.

Bibliography

[1] Battery degradation and power loss. http://www.batteryeducation.com/2006/04/battery_degrada.html, 2006.

[2] Chargecar project website. http://www.chargecar.org, 2012.

[3] hybrid battery fan cleaning toyota prius hybrid (hv battery fan traction battery fan). http://www.youtube.com/channel/UCBZVtBqF4pfNIEqo4s00KvQ, 2015.

[4] Direct and indirect cooling systems. http://ref-wiki.com/technical-information/148-evaporators/32656-direct-and-indirect-cooling-systems.html, 2016.

[5] Direct vs. indirect. http://www.glesolar.com/solar-basics/why-gle-solar-energy/direct-vs-indirect, 2016.

[6] Evaporator. http://www.airconditioning-systems.com/evaporator.html, 2016.

[7] Fluid properties calculator. http://www.mhtl.uwaterloo.ca/old/onlinetools/airprop/airprop.html, 2016.

[8] fmincon. http://www.mathworks.com/help/optim/ug/fmincon.html, 2016.

[9] fminsearch. http://www.mathworks.com/help/matlab/ref/fminsearch.html, 2016.

[10] Ftp-75. https://en.wikipedia.org/wiki/FTP-75, 2016.

[11] Fundamentals of active vs. passive thermal management. http://www.electronicproducts.com/Thermal_Management/Heat_Sinks_and_Thermal_Materials/Fundamentals_of_active_vs_passive_thermal_management.aspx, 2016.

[12] How can lithium-ion batteries improve hybrids? http://auto.howstuffworks.com/lithium-ion-batteries-improve-hybrids1.htm, 2016.

[13] Hybrid training: Hybrid battery cooling systems video. https://www.youtube.com/watch?v=JXp_3Awb-SQ, 2016.

[14] Quadratic programming problems- a review on algorithms and applications (active-set and interior point methods). https://www.tu-ilmenau.de/fileadmin/media/simulation/Lehre/Vorlesungsskripte/Lecture_materials_Abebe/QPs_with_IPM_and_ASM.pdf, 2016.

[15] Said Al Hallaj, Hossein Maleki, Jong-Sung Hong, and J Robert Selman. Thermal modeling and design considerations of lithium-ion batteries. *Journal of power sources*, 83(1):1–8, 1999.

[16] Nasser L Azad, Ahmad Mozaffari, Mahyar Vajedi, and Yasaman Masoudi. Chaos oscillator differential search combined with pontryagins minimum principle for simultaneous power management and component sizing of phevs. *Optimization and Engineering*, pages 1–34.

[17] Nasser L Azad, Ahmad Mozaffari, Mahyar Vajedi, and Yasaman Masoudi. Chaos oscillator differential search combined with pontryagins minimum principle for simultaneous power management and component sizing of phevs. *Optimization and Engineering*, pages 1–34.

[18] Marko Bacic. On hardware-in-the-loop simulation. In *Proceedings of the 44th IEEE Conference on Decision and Control*, pages 3194–3198. IEEE, 2005.

[19] Robb A Barnitt, Aaron D Brooker, Laurie Ramroth, John Rugh, and Kandler A Smith. Analysis of off-board powered thermal preconditioning in electric drive vehicles. *National Renewable Energy Laboratory, Golden, CO*, 2010.

[20] Sebastian Bauer, Andre Suchaneck, and Fernando Puente León. Thermal and energy battery management optimization in electric vehicles using pontryagin's maximum principle. *Journal of Power Sources*, 246:808–818, 2014.

[21] Alberto Bemporad. Model predictive control design: New trends and tools. In *Proceedings of the 45th IEEE Conference on Decision and Control*, pages 6678–6683. IEEE, 2006.

[22] Michael Benz, Markus Hehn, Christopher H Onder, and Lino Guzzella. Model-based actuator trajectories optimization for a diesel engine using a direct method. *Journal of Engineering for Gas Turbines and Power*, 133(3):032806, 2011.

[23] Theodore L Bergman, Frank P Incropera, David P DeWitt, and Adrienne S Lavine. *Fundamentals of heat and mass transfer*. John Wiley & Sons, 2011.

[24] Theodore L Bergman, Frank P Incropera, David P DeWitt, and Adrienne S Lavine. *Fundamentals of heat and mass transfer*. John Wiley & Sons, 2011.

[25] Lorenz T Biegler. Nonlinear programming strategies for dynamic chemical process optimization. *Theoretical Foundations of Chemical Engineering*, 48(5):541–554, 2014.

[26] H Ali Borhan, Ardalan Vahidi, Anthony M Phillips, Ming L Kuang, and Ilya V Kolmanovsky. Predictive energy management of a power-split hybrid electric vehicle. In *2009 American control conference*, pages 3970–3976. IEEE, 2009.

[27] Hoseinali Borhan, Ardalan Vahidi, Anthony M Phillips, Ming L Kuang, Ilya V Kolmanovsky, and Stefano Di Cairano. Mpc-based energy management of a power-split hybrid electric vehicle. *IEEE Transactions on Control Systems Technology*, 20(3):593–603, 2012.

[28] F Borrelli, A Bemporad, and M Morari. Predictive control for linear and hybrid systems. 2014. *preparation, available online at http://www. mpc. berkeley. edu/mpc-course-material*.

[29] Francesco Borrelli, Paolo Falcone, Tamas Keviczky, Jahan Asgari, and Davor Hrovat. Mpc-based approach to active steering for autonomous vehicle systems. *International Journal of Vehicle Autonomous Systems*, 3(2-4):265–291, 2005.

[30] Alain Bouscayrol. Different types of hardware-in-the-loop simulation for electric drives. In *2008 IEEE International Symposium on Industrial Electronics*, pages 2146–2151. IEEE, 2008.

[31] Stephen Boyd and Lieven Vandenberghe. *Convex optimization*. Cambridge university press, 2004.

[32] S Di Cairano, Alberto Bemporad, IV Kolmanovsky, and Davor Hrovat. Model predictive control of magnetically actuated mass spring dampers for automotive applications. *International Journal of Control*, 80(11):1701–1716, 2007.

[33] Dafen Chen, Jiuchun Jiang, Gi-Heon Kim, Chuanbo Yang, and Ahmad Pesaran. Comparison of different cooling methods for lithium ion battery cells. *Applied Thermal Engineering*, 94:846–854, 2016.

[34] Stefano Di Cairano and H Eric Tseng. Driver-assist steering by active front steering and differential braking: design, implementation and experimental evaluation of a switched model predictive control approach. In *49th IEEE Conference on Decision and Control (CDC)*, pages 2886–2891. IEEE, 2010.

[35] Paolo Falcone, Francesco Borrelli, Jahan Asgari, Hongtei Eric Tseng, and Davor Hrovat. Predictive active steering control for autonomous vehicle systems. *IEEE Transactions on control systems technology*, 15(3):566–580, 2007.

[36] Hosam K Fathy, Zoran S Filipi, Jonathan Hagena, and Jeffrey L Stein. Review of hardware-in-the-loop simulation and its prospects in the automotive area. In *Defense and Security Symposium*, pages 62280E–62280E. International Society for Optics and Photonics, 2006.

[37] Hans Joachim Ferreau, Peter Ortner, Peter Langthaler, Luigi Del Re, and Moritz Diehl. Predictive control of a real-world diesel engine using an extended online active set strategy. *Annual Reviews in Control*, 31(2):293–301, 2007.

[38] Roger Fletcher. *Practical methods of optimization*. John Wiley & Sons, 2013.

[39] Carlos E Garcia, David M Prett, and Manfred Morari. Model predictive control: theory and practicea survey. *Automatica*, 25(3):335–348, 1989.

[40] Abib Geletu. Quadratic programming problems- a review on algorithms and applications, October 8 2011.

[41] L. Grüne and J. Pannek. *Nonlinear Model Predictive Control: Theory and Algorithms*. Communications and Control Engineering. Springer London, 2011.

[42] WB Gu and Chao-Yang Wang. Thermal and electrochemical coupled modeling of a lithium-ion cell. *Proc.-Electrochem. Soc*, 99:748–762, 2000.

[43] Lino Guzzella, Antonio Sciarretta, et al. *Vehicle propulsion systems*, volume 1. Springer, 2007.

[44] TD Hatchard, DD MacNeil, A Basu, and JR Dahn. Thermal model of cylindrical and prismatic lithium-ion cells. *Journal of The Electrochemical Society*, 148(7):A755–A761, 2001.

[45] Hongwen He, Rui Xiong, and Jinxin Fan. Evaluation of lithium-ion battery equivalent circuit models for state of charge estimation by an experimental approach. *Energies*, 4(4):582–598, 2011.

[46] K Hinderer. The principle of optimality and the optimality equation. In *Foundations of Non-stationary Dynamic Programming with Discrete Time Parameter*, pages 14–27. Springer, 1970.

[47] Theo Hofman, RM van Druten, M Steinbuch, and AFA Serrarens. Rule-based equivalent fuel consumption minimization strategies for hybrid vehicles. *IFAC Proceedings Volumes*, 41(2):5652–5657, 2008.

[48] Ronald H.W. Hoppe. Chapter 3, quadratic programming. https://www.math.uh.edu/~rohop/fall_06/Chapter3.pdf, 2016.

[49] Xiaosong Hu, Nikolce Murgovski, Lars Mårdh Johannesson, and Bo Egardt. Comparison of three electrochemical energy buffers applied to a hybrid bus powertrain with simultaneous optimal sizing and energy management. *IEEE Transactions on Intelligent Transportation Systems*, 15(3):1193–1205, 2014.

[50] Xiaosong Hu, Nikolce Murgovski, Lars Mårdh Johannesson, and Bo Egardt. Optimal dimensioning and power management of a fuel cell/battery hybrid bus via convex programming. *IEEE/ASME transactions on mechatronics*, 20(1):457–468, 2015.

[51] Yiran Hu, S Yurkovich, Y Guezennec, and BJ Yurkovich. Electro-thermal battery model identification for automotive applications. *Journal of Power Sources*, 196(1):449–457, 2011.

[52] Y Inui, Y Kobayashi, Y Watanabe, Y Watase, and Y Kitamura. Simulation of temperature distribution in cylindrical and prismatic lithium ion secondary batteries. *Energy Conversion and Management*, 48(7):2103–2109, 2007.

[53] Nashat Jalil, Naim A Kheir, and Mutasim Salman. A rule-based energy management strategy for a series hybrid vehicle. In *American Control Conference, 1997. Proceedings of the 1997*, volume 1, pages 689–693. IEEE, 1997.

[54] Kenneth J Kelly, Mark Mihalic, and Matthew Zolot. Battery usage and thermal performance of the toyota prius and honda insight during chassis dynamometer testing. In *Battery Conference on Applications and Advances, 2002. The Seventeenth Annual*, pages 247–252. IEEE, 2002.

[55] Eugene Kim, Kang G Shin, and Jinkyu Lee. Real-time battery thermal management for electric vehicles. In *ICCPS'14: ACM/IEEE 5th International Conference on Cyber-Physical Systems (with CPS Week 2014)*, pages 72–83. IEEE Computer Society, 2014.

[56] Gi-Heon Kim and Ahmad Pesaran. *Battery thermal management system design modeling*. National Renewable Energy Laboratory, 2006.

[57] Donald E Kirk. *Optimal control theory: an introduction*. Courier Corporation, 2012.

[58] Michiel Koot, John TBA Kessels, Bram de Jager, WPMH Heemels, PPJ Van den Bosch, and Maarten Steinbuch. Energy management strategies for vehicular electric power systems. *IEEE transactions on vehicular technology*, 54(3):771–782, 2005.

[59] Fred Lambert. electrek news site. https://electrek.co/2016/08/01/gm-100000th-chevy-volt-us-1-5-billion-electric-miles, 2016.

[60] Energy Storage Task Lead and Ahmad Pesaran. Battery thermal modeling and testing.

[61] Julien Lescot, Antonio Sciarretta, Yann Chamaillard, and Alain Charlet. On the integration of optimal energy management and thermal management of hybrid electric vehicles. In *2010 IEEE Vehicle Power and Propulsion Conference*, pages 1–6. IEEE, 2010.

[62] Chan-Chiao Lin, Huei Peng, Jessy W Grizzle, and Jun-Mo Kang. Power management strategy for a parallel hybrid electric truck. *IEEE transactions on control systems technology*, 11(6):839–849, 2003.

[63] Yue Ma, Ho Teng, and Marina Thelliez. Electro-thermal modeling of a lithium-ion battery system. *SAE International Journal of Engines*, 3(2010-01-2204):306–317, 2010.

[64] Andreas A Malikopoulos. Supervisory power management control algorithms for hybrid electric vehicles: a survey. *IEEE Transactions on intelligent transportation systems*, 15(5):1869–1885, 2014.

[65] Yasaman Masoudi, Ahmad Mozaffari, and Nasser L Azad. Battery thermal management of electric vehicles: An optimal control approach. In *ASME 2015 Dynamic Systems and Control Conference*, pages V001T13A003–V001T13A003. American Society of Mechanical Engineers, 2015.

[66] D.Q. Mayne, J.B. Rawlings, C.V. Rao, and P.O.M. Scokaert. Constrained model predictive control: Stability and optimality. *Automatica*, 36(6):789 – 814, 2000.

[67] Scott J. Moura. *Techniques for Battery Health Conscious Power Management via Electrochemical Modeling and Optimal Control*. PhD thesis, 2011.

[68] GJL Naus, Jeroen Ploeg, MJG Van de Molengraft, WPMH Heemels, and Maarten Steinbuch. Design and implementation of parameterized adaptive cruise control: An explicit model predictive control approach. *Control Engineering Practice*, 18(8):882–892, 2010.

[69] Pu-yan Nie. A null space method for solving system of equations. *Applied Mathematics and computation*, 149(1):215–226, 2004.

[70] Kevin Kenneth Parsons. *Design and Simulation of Passive Thermal Management System for Lithium-Ion Battery Packs on an Unmanned Ground Vehicle*. PhD thesis, California Polytechnic State University, San Luis Obispo, 2012.

[71] Ahmad Pesaran, Tony Markel, Harshad S Tataria, and David Howell. Battery requirements for plug-in hybrid electric vehicles: analysis and rationale. In *23 rd International Electric Vehicle Symposium*, pages 2–5, 2007.

[72] Ahmad A Pesaran. Battery thermal management in ev and hevs: issues and solutions. *Battery Man*, 43(5):34–49, 2001.

[73] Ahmad A Pesaran. Battery thermal models for hybrid vehicle simulations. *Journal of Power Sources*, 110(2):377–382, 2002.

[74] Ahmad A Pesaran, Steve Burch, and Matthew Keyser. An approach for designing thermal management systems for electric and hybrid vehicle battery packs. *4th Vehicle Thermal Management Systems*, pages 24–27, 1999.

[75] TH Pham, PPJ van den Bosch, JTBA Kessels, and RGM Huisman. Cost-effective energy management for hybrid electric heavy-duty truck including battery aging. In *ASME 2013 Dynamic Systems and Control Conference*, pages V001T05A001–V001T05A001. American Society of Mechanical Engineers, 2013.

[76] Reza Sharif Razavian, Nasser L Azad, and John McPhee. A battery hardware–in–the–loop setup for concurrent design and evaluation of real–time optimal hev power management controllers. *International Journal of Electric and Hybrid Vehicles*, 5(3):177–194, 2013.

[77] Ehsan Samadani. *Modeling of Lithium-ion Battery Performance and Thermal Behaviour in Electrified Vehicles*. PhD thesis, University of Waterloo, Waterloo, 2015.

[78] Shriram Santhanagopalan, Kandler Smith, Jeremy Neubauer, Gi-Heon Kim, Ahmad Pesaran, and Matthew Keyser. *Design and Analysis of Large Lithium-Ion Battery Systems*. Artech House, 2014.

[79] Antonio Sciarretta, Michael Back, and Lino Guzzella. Optimal control of parallel hybrid electric vehicles. *IEEE Transactions on control systems technology*, 12(3):352–363, 2004.

[80] Antonio Sciarretta and Lino Guzzella. Control of hybrid electric vehicles. *IEEE Control systems*, 27(2):60–70, 2007.

[81] Mojtaba Shams-Zahraei, Abbas Z Kouzani, Steffen Kutter, and Bernard Bäker. Integrated thermal and energy management of plug-in hybrid electric vehicles. *Journal of power sources*, 216:237–248, 2012.

[82] Ying Shi, Kandler Smith, Eric Wood, and Ahmad Pesaran. A multi-node thermal system model for lithium-ion battery packs. In *2015 American Control Conference (ACC)*, pages 723–727. IEEE, 2015.

[83] Kang G Shin and Eugene Kim. Real-time battery thermal management for electric vehicles, October 1 2015. US Patent 20,150,280,294.

[84] Phani B Sistu and B Wayne Bequette. Nonlinear model-predictive control: Closed-loop stability analysis. *AIChE Journal*, 42(12):3388–3402, 1996.

[85] Marco Sorrentino, Gianfranco Rizzo, and Ivan Arsie. Analysis of a rule-based control strategy for on-board energy management of series hybrid vehicles. *Control Engineering Practice*, 19(12):1433–1441, 2011.

[86] Stephanie Stockar, Vincenzo Marano, Giorgio Rizzoni, and Lino Guzzella. Optimal control for plug-in hybrid electric vehicle applications. In *Proceedings of the 2010 American control conference*, pages 5024–5030. IEEE, 2010.

[87] Toyota Information System. *Hybrid/battery control: hybrid control system: details 2015 My Prius PHV,Doc ID: RM000004273OOMX*. 2015.

[88] Peyman Taheri and Majid Bahrami. Temperature rise in prismatic polymer lithium-ion batteries: An analytic approach. *SAE International Journal of Passenger Cars-Electronic and Electrical Systems*, 5(2012-01-0334):164–176, 2012.

[89] Sadegh Tajeddin, Mahyar Vajedi, and Nasser L Azad. A newton/gmres approach to predictive ecological adaptive cruise control of a plug-in hybrid electric vehicle in car-following scenarios. *IFAC-PapersOnLine*, 49(21):59–65, 2016.

[90] Xinran Tao, Kan Zhou, Andrej Ivanco, John R Wagner, Heath Hofmann, and Zoran Filipi. A hybrid electric vehicle thermal management system-nonlinear controller design. In *SAE International*, 2015.

[91] Xinran William Tao and John Wagner. Cooling air temperature and mass flow rate control for hybrid electric vehicle battery thermal management. In *ASME 2014 Dynamic Systems and Control Conference*, pages V002T34A002–V002T34A002. American Society of Mechanical Engineers, 2014.

[92] Xinran William Tao and John Wagner. Cooling air temperature and mass flow rate control for hybrid electric vehicle battery thermal management. In *ASME 2014 Dynamic Systems and Control Conference*, pages V002T34A002–V002T34A002. American Society of Mechanical Engineers, 2014.

[93] Mahyar Vajedi. *Real-time Optimal Control of a Plug-in Hybrid Electric Vehicle Using Trip Information*. PhD thesis, 2016.

[94] Mahyar Vajedi, Maryyeh Chehrehsaz, and Nasser L Azad. Intelligent power management of plug–in hybrid electric vehicles, part ii: real–time route based power management. *International Journal of Electric and Hybrid Vehicles*, 6(1):68–86, 2014.

[95] Xi Wei, L Guzzella, VI Utkin, and G Rizzoni. Model-based fuel optimal control of hybrid electric vehicle using variable structure control systems. *Journal of dynamic systems, measurement, and control*, 129(1):13–19, 2007.

[96] Li Xu, H Eric Tseng, and Davor Hrovat. Hybrid model predictive control of active suspension with travel limits and nonlinear tire contact force. In *American Control Conference (ACC), 2016*, pages 2415–2420. American Automatic Control Council (AACC), 2016.

[97] Fengjun Yan, Junmin Wang, and Kaisheng Huang. Hybrid electric vehicle model predictive control torque-split strategy incorporating engine transient characteristics. *IEEE Transactions on Vehicular Technology*, 61(6):2458–2467, 2012.

[98] Tugce Yuksel and Jeremy Michalek. Development of a simulation model to analyze the effect of thermal management on battery life. Technical report, SAE Technical Paper, 2012.

[99] Tugce Yuksel and Jeremy J Michalek. Evaluation of the effects of thermal management on battery life in plug-in hybrid electric vehicles. 2012.

[100] Victor M Zavala and Lorenz T Biegler. The advanced-step nmpc controller: Optimality, stability and robustness. *Automatica*, 45(1):86–93, 2009.

[101] Matthew Zolot, Ahmad A Pesaran, and Mark Mihalic. Thermal evaluation of toyota prius battery pack. Technical report, SAE Technical Paper, 2002.

[102] Matthew D Zolot, K Kelly, M Keyser, M Mihalic, A Pesaran, and A Hieronymus. Thermal evaluation of the honda insight battery pack. In *Intersociety Energy Conversion Engineering Conference*, volume 2, pages 923–928. SAE; 1999, 2001.